T.C.

AYDIN ADNAN MENDERES UNIVERSITY

GRADUATE SCHOOL OF NATURAL AND APPLIED SCIENCES

MASTER'S PROGRAMME IN CIVIL ENGINEERING

THE EFFECTS OF HAIL IMPACT ON STEEL ROOFING PROFILES WITH FEM AND LABORATORY TESTS

MERYEM DILARA KOP

MASTER'S THESIS

SUPERVISOR

Dr. Mehmet Eren UZ

AYDIN-2022

ACCEPTANCE AND APPROVAL

The thesis titled “The Effects of Hail Impact on Steel Roofing Profiles with FEM and Laboratory Tests”, prepared by Meryem Dilara KOP, a student of Department of Civil Engineering at Aydin Adnan Menderes University, was accepted as a Master's Thesis by the jury below.

Date of Thesis Defence: 02/08/2022

Title, Name Surname		University	Signature
Member (T.D):	.....	.....	
Member:	.....	.....	
Member:	.....	.....	

APPROVAL:

This thesis was approved by the jury above in accordance with the relevant articles of the Aydın Adnan Menderes University Graduate Education and Examination Regulations and was approved on the .....by from the Board of Directors of the Graduate School of Science in the .....numbered decision

……

Institute Director

ACKNOWLEDGEMENTS

In this thesis, my supervisor Dr. Mehmet Eren UZ guided me. My thesis and my master's degree supported with his knowledge and experiences. For all his support, I would like to thank him.

During this study, Gökalp YILMAZ helped me in research and experiments who is a Master degree student in Department of Mechanical Engineering. Endless thanks to Mohammad Dawood SIZAR and Efe Mert Yıldırm for their help.

Supports and Beliefs of my family and friends are significant to me. They always sustain me to do the best I can. That feels in confident in my education life. For this feeling, I always be grateful.

TABLE OF CONTENTS

LIST OF SYMBOLS AND ABBREVIATIONS

α and **β** : They are the coefficients for the rebounded energy and the compressive area, respectively

D(gauge) : Dent depth measured by dent caliper

D (Proposed) : Dent depth calculated by proposed equation

D (FEM) : Dent Depth obtained from Finite elemement model

***COR*:** **:** Coefficient of Restitution

x: **:** The compressive distance under sinusodial steady-state response

w : **:** The external frequency of artificial hailstone

k **:** The flexural stiffness of the flat sheet

h **:** Transversal length

c **:** Dent depth (D)

a and **b** **:** They are equal to the elliptic dented radius (r)

φ **:** Diameter of the artificial hailstone (2R)

ϰ: **:** The coefficient

V **:** Impact velocity in equation

t **:** Thickness of the plate.

r **:** Radius of siplified dented area before the impact

R **:** Radius of artificial hailstone

PVA **:** Polivinil Alcohol

N_2 **:** Molecular formulation of Liquid Nitrogen

N **:** Chemical Symbol of Nitrogen

m **:** Mass of the artificial hailstone

l **:** Spacing between battens

F **:** Force

E **:** Young's modulus

$\Delta \mathbf{A}$: Change of the area.

$\boldsymbol{\omega_n}$: : Natural frequency

$\boldsymbol{\sigma_y}$: : Yield Stress of Plate

$\boldsymbol{V_s}$: Velocity obtained from sensors

$\boldsymbol{V_c}$: Velocity calculated from high-speed camera

$\boldsymbol{V_a}$: Average velocity of hailstone

$\mathbf{R_c}$: Compressive radius

$\mathbf{E_{Vibration}}$: : Energy of vibration

$\mathbf{E_{Rebound}}$: : Rebound Energy

$\mathbf{E_{Plastic}}$: : Plastic Energy

$\mathbf{E_{Impact}}$: : Impact Energy

$\mathbf{D_d}$: Dent diameter

$\mathbf{A_0}$: : The original dent area

$\mathbf{A_f}$: : The deformed area

$\Delta \mathbf{A_r}$: Revised changed area

$\left|\mathbf{H_{jw}}\right|$: : The dynamic amplification factor

LIST OF FIGURES

LIST OF TABLES

ÖZET

DOLU DARBESİNİN ÇELİK ÇATI PROFİLLERİNE SONLU ELEMEANLAR YÖNTEMİ (FEM) VE LABORATUVAR TESTLERİ İLE ETKİLERİ

KOP M. D. Aydın Adnan Menderes Üniversitesi, Fen Bilimleri Enstitüsü, İnşaat Mühendisliği Programı, Yüksek Lisans Tezi, Aydın, 2022

Amaç: Bu çalışmada çelik panel üzerindeki göçük derinliğinin incelenmesi amaçlanmaktadır. Göçük derinliğini tahmin etmek için önerilen denklem çalışmanın sonunda sunulmuştur.

Materyal ve Yöntem: Bu çalışmada suni dolu üretiminde yeni yöntem kullanılmıştır. Literatürde, suni dolu yapmak için çeşitli yöntemler vardır. Şimdiye kadar, farklı malzemeler buzun çekme mukavemetini arttırmak için kullanılmıştır. En yaygın yöntem, PVA'yı (polivinil alkol) yapıştırıcı olarak kullanmaktır. Deneysel testlerde, suni dolu taneleri sıvı PVA yapıştırıcı ile demineralize sudan ve sıvı azot ile demineralize sudan yapılır. Darbe testleri bu suni dolu taneleri ile yapılmaktadır. Hedefteki göçük derinliğini tahmin etmek için önerilen denklem kullanılır. Suni doluyu simüle etmek için sonlu elemanlar modeli de geliştirilmiştir. Deneyde, dinamik dolu darbe testleri için 0.35, 0.45, 0.60, 0.70, 0.80 ve 1 mm kalınlığındaki G300 çelik saclar kullanılmıştır. Laboratuvarda üç farklı çapta suni dolu tanesi üretilmektedir. Bu çaplar 38, 45 ve 50 mm'dir. Bu yapay dolu taneleri, farklı kalınlıklardaki çelik saclarla dinamik darbe testinde de kullanılmaktadır.

Bulgular: Dinamik darbe testi iki farklı türde suni dolu için gerçekleştirilmiştir. Biri %12 PVA ve %88 demineralize sudan, diğeri ise sıvı azot ve demineralize sudan oluşur. Önerilen denklem, göçük derinliğini tahmin etmek için sunuldu. Teorik deneylerin sonuçları ve sonlu elemanlar modeli sunulmuştur. Darbe testlerine göre, sıvı azot ve demineralize sudan yapılmış suni dolu tanelerinin, doğal dolu tanesinin yapısına ve davranışına benzerlik göstermektedir.

Sonuç: Bu çalışmaya göre, önerilen denklem, darbe enerjisinin, plaka kalınlığının, malzeme kalınlığının, Tahtaların arasındaki mesafenin, göçük ağırlık merkezinin plakanın en yakın kenarından uzaklığının ve dolu çapının göçük derinliğini etkileyen parametreler olduğunu göstermektedir. Sıvı azot kullanımı, doğal dolunun yapısını oluşturmada rol oynar.

Anahtar Kelimeler: Sıvı Nitrojen, Suni Dolu, Dinamik Darbe Testi, Göçük Derinliği.

ABSTRACT

THE EFFECTS OF HAIL IMPACT ON STEEL ROOFING PROFILES WITH FEM AND LABORATORY TESTS

KOP M. D. Aydin Adnan Menderes University, Graduate School of Natural and Applied Science, Civil Engineering Program, Master's Thesis, Aydin, 2022

Objective: The purpose of this study is to investigate the dent depth on the steel sheet. To predict the dent depth, the proposed equation was presented at the end of the study.

Material and Methods: In this work, the new method for producing artificial hailstone was used. In the literature, there are various methods for making artificial hailstone. So far, different materials have been used to increase the tensile strength of the ice. The most common method is to use PVA (polyvinyl alcohol) as an adhesive. In the experimental tests, artificial hailstones are made from liquid PVA adhesive and demineralised water, and from liquid nitrogen and demineralised water. Impact tests are conducted with these artificial hailstones. The proposed equation is used to predict the dent depth on the target. A finite element model was also developed to simulate the artificial hailstone. In the experiment, 0.35, 0.45, 0.60, 0.70, 0.80 and 1 mm thick G300 steel sheets are used for the dynamic hail impact tests. In the laboratory, artificial hailstones with three different diameters are produced. These diameters are 38, 45 and 50 mm. These artificial hailstones are also used in the dynamic impact test with steel sheets of different thicknesses.

Results: The dynamic impact test was carried out for two different types of artificial hailstones. One consists of 12% PVA and 88% demineralised water and the other of liquid nitrogen and demineralised water. The proposed equation was presented to predict the dent depth. The results of the theoretical experiments and the finite element model are presented. According to the impact tests, artificial hailstones made of liquid nitrogen and demineralised water are able to imitate the structure and behaviour of the natural hailstone.

Conclusion: According to this study, the proposed equation shows that the impact energy, the plate thickness, the material thickness, the distance between the battens, the distance of the dent centre of gravity from the nearest edge of the plate and the hail diameter are the parameters that influence the dent depth. The use of liquid nitrogen plays a role in creating the structure of the natural hailstone.

Keywords: Liquid Nitrogen, Artificial Hailstone, Dynamic Impact test, Dent depth.

1. INTRODUCTION

Hail can cause damage amounting to millions. The situation of roofs during hailstorms is important because roofs are exposed to the worst weather conditions and any damage to roofs affects buildings. It has been proven that hailstorms can cause significant damage to roofs. Due to low maintenance costs and better resistance to natural disasters, steel roofs are becoming increasingly popular (Wu, 2018). In 1999, Sydney was hit by a hailstorm that caused a total insurance loss of $1.7 billion, damaged 20,000 roofs and affected over 13,000 people. Figure 1 shows the hailstones that damaged a vehicle in Turkey on 27 July 2017. 180 thousand vehicles were affected by the hailstorm. On 29 September 2020, a hailstorm caused 150 million TL worth of damage.

Figure 1. Damage caused by hailstones to a vehicle Source: https://www.cnnturk.com/

Depending on the air flow, the diameter of the hailstones may be higher than 45 mm (the size of a golf ball). Depending on the current climate change trends, the prediction is that the number of a hailstorm will increase in the future (Leslie et al., 2008). Climate change is predicted to result in an increase in hailstorms in the future. According to Australian climate models, hail days will increase by one to two days by 2030 and by four to six days by 2070 (CSIRO and BoM, 2007). Brimelow et al. (2002) examined the spatial and temporal differences in hail dimensions and frequency over two 30-year time periods, 1971-2000 and 2041-2070.

Due to climate change, the average size of hailstones is expected to increase. In addition, hailstorms are expected to increase in Australia and Europe while decreasing in Asia and North America. This increase in hail diameters will make existing roofs even more vulnerable (Raupach et al., 2021). An example of damage to a roof can be found in Figure 2.

Figure 2. An example of a roof panel that has been damaged by hail Source: https://royalroofinginc.com/

The direct and indirect damage caused by hailstorms shows that hail damage to roofs is not negligible. Despite the fact that hail can cause extensive damage to roofs, there is a lack of literature on the effects of hail on roofs. It is difficult to detect hail damage to roofs when there are no leaks or physical damage. For hailstones to cause significant damage after impact, it is important that they remain intact after impact at relatively high velocities.

In order to accurately assess hail damage to exposed roofing materials, the natural behaviour of hailstones upon impact must be simulated. The first step in this study is to produce artificial hailstones that remain intact after impact in order to subsequently investigate the damage to the steel roof. Once the artificial hailstone has passed the impact test by being applied to steel sheets, a formula will be developed to predict the dent depth.

2. LITERATURE REVIEW

This section of the thesis provides an overview of the hail simulation studies conducted to date. A variety of materials and methods have been used to produce artificial hailstone and numerical models have been developed to study the hailstone.

Initially, Niemeier and Burley (1978) investigated the hail resistance of roofing materials under real hailstorms. However, this method had some limitations, including the following:

- To determine the correlation between the size of the hailstone and the damage caused by the impacting hailstone
- Natural hailstone collection

Johnson and Schaffnit (1973), Nomura et al. (1984), Fleming et al. (1997) and Shi et al. (1997) used steel indenters for impact tests. In the impact test conducted by Vreede et al. (1995), steel balls were dropped from a certain distance to obtain the same kinetic energy developed by Laurie (1960) However, the impact damage caused by steel balls or other indentors is different from that caused by hailstones.

Using Polyamide balls and ice balls made from demineralized water, Flüeler et al. (2008) conducted impact experiments. There have been studies conducted using ice balls made from tap water by Greenfeld (1969), Kim and Kedward (1999), Kim et al. (2003), Juntikka and Olsson (2009), Chang and Khetan (1984), and Paterson and Sankaran (1994). By combining a certain temperature and pressure with tap water, Moore and Wilson (1978) produced artificial hailstones. Artificial hailstones failed to represent intact conditions following the impact test.

The flat-wise layered structure method was used by Kim et al. (2003) and Flüeler et al. (2008) to produce artificial hailstones. The method was also used by Tippmann (2011). Natural hailstone has an onion-shaped structure, while artificial hailstone produced by this method has a layered structure. Because of this difference, the artificial hailstones do not remain intact after impact tests.

Schulson (1999) produced artificial hailstones by immersing demineralized water and solid carbon dioxide in water. Using this method, onion layers were layered, but the shape was an irregular oval rather than a sphere, since it was difficult to control. In the outer layer of the

ice, carbon dioxide is present, which weakens the ice, causing the hailstones to be crushed during the impact test as a result.

Allaby and Garratt (2014) produced artificial hailstones using distilled water. Unlike previous studies, the first embryo was created using dry ice in an immersion process. It was then applied to a ping-pong ball with a hole at the top. Boiled distilled water is poured into the ping pong ball through this hole. The result of this process was a perfectly spherical shape with a clear outer layer. The researchers found that none of the hailstones were perfectly spherical and one out of twelve artificial hailstones remained intact.

Similarly to the previous study, Liang (2015) and Ramsay (2015) produced artificial hailstones by boiling deionised water. It was possible to create some hailstones that remained intact after impacting at a certain velocity. According to the authors, the ice balls should be free of cracks and air. Nevertheless, the first impact tests were not successful due to cracks and air inclusions. By increasing the strength of an ice sphere, the ice sphere remains intact after impact. The ice was 14% sawdust and 86% water, which is known as pykrete. It is important to note that pykrete increases tensile strength in a very different way than ice made by Gold (2014).

The addition of cotton fibres or polypropylene fibres can also increase the tensile strength of ice balls (Ramsay, 2015; Tippmann, 2011). According to Swift (2013), cotton increases extensibility. In initial impact tests, some artificial hailstones remained intact, but as the speed increased, the artificial hailstones no longer showed the same integrity.

According to Wu (2018), the addition of PVA-based adhesive and microfibres to artificial hailstones does not significantly alter their other physical properties. Wu (2018) conducted impact tests using 0.55 mm thick G300 steel sheets with an average impact velocity of 30 m/s. The results of the experiment showed that only 12% PVA and 88% demineralised water passed.

A correlation between the dent depth and impact energy was found by Wu (2018), consistent with Worswick et al. (1997). PVA is believed to provide hailstones with similar performance to rubber. However, an assumption is that such hailstones cannot mimic the response of natural hailstones, which do not break on impact. The addition of PVA makes the hail behave like rubber. As can be seen in Figure 3, a special waste is produced after the melting process.

Figure 3. An image of a water-based artificial hailstone containing 12% PVA material after melting

A new method for producing artificial hailstone was developed by Yilmaz et al. (2020) found a new method to make artificial hailstone. According to the authors, the artificial hailstone used so far cannot successfully simulate hailstone. To produce artificial hailstone, Yilmaz et al. (2020) used liquid nitrogen and demineralised water, a method that has not been used before. In this study, dynamic impact tests were conducted with hailstones made of 12% PVA and liquid nitrogen. G300 steel sheets were used for the impact tests. The results of the experiments indicate that liquid nitrogen hailstones are more likely to remain intact after impact.

In this thesis, two different methods of producing artificial hailstones are presented. One uses liquid nitrogen and demineralised water. Another method uses 12% PVA and 88% demineralised water. The use of liquid nitrogen is a new method in the literature. These two types of artificial hailstones were subjected to dynamic impact tests. G300 steel sheets are used for the dynamic impact tests. After impact, artificial hailstones made of liquid nitrogen and demineralised water remain intact to a high percentage, but with a slightly higher terminal velocity. Hailstones made of liquid nitrogen and demineralised water have properties similar to those of natural hailstones. The use of steel balls, penetrators and normal ice balls in previous studies failed to demonstrate the properties and impact damage of natural hailstones. In impact tests, the liquid nitrogen hailstone did not break, and other parameters, such as density, were very similar to those of natural hailstone. Because of these factors, it is possible to reduce implementation costs without increasing the thickness of the roof panel. Roof coverings come in a variety of types.

The aim of this study is to investigate the buckling resistance of metal roofs. The advantages of metal roofs include their long life, low cost and light weight. Generally, hailstorms cause visible damage to metal roofs, which is called cosmetic damage. There is a possibility that indentations may cause ponding and dirt accumulation, which can eventually lead to corrosion. According to current knowledge, there is no uniform method for predicting the dimensions of an indentation caused by hail.

3. MATERIAL AND METHOD

Heymsfield et al. (2020) studied the terminal velocity of spherical hailstones. Usually, hailstorm tests are performed by propelling or dropping placeholder hailstones of different sizes, shapes and weights at different velocities. In this work, test devices capable of performing different impact tests, 0.30 mm, 0.45 mm, 0.6 mm, 0.7 mm, 0.80 mm and 1 mm G300 steel sheets, and a proposed equation for predicting the dent depth were evaluated in this thesis.

3.1. Hailstone Behavior and Properties

The structure of ice is complex. There are many fascinating aspects of hail growth that can be explored. According to Dunlop (2008), a hailstone is defined as a ball of ice larger than 5 millimetres in diameter. Due to the fact that hailstones contain water, they have some similarities with ice. The behaviour and properties of hailstones have been studied by a variety of researchers.

In addition to the size of the hailstones, upwind conditions such as upwind speed and temperature, as well as the amount of liquid water in the clouds, also play an important role in the accretion rate and the type of growth of the hailstones (Brimelow, 2018).

In the center of hail there is an embryo. Laurie (1960) explains that the embryo is composed of salt, dust, and other particles. The number of frozen drop embryos tends to increase in proportion to the size of the hail. With an increase in this factor, opaque layers can become clear. When hail is transported to a different temperature zone within clouds, it is made stronger and more elastic due to these layers and crystal structure (Hile, 2009; Oard, 2015).

In the past, artificial hailstones were made by freezing the outside. When the core freezes, the air collects on the outer shell. About 75 percent of hailstones in nature have a spherical shape and their density is between 700 and 920 kg/m^3.

In general, hail has a bulk density closest to that of frozen water (i.e., about 900 kg/m^3) (Brimelow, 2018). Natural hailstones can have a wide range of compressive strength values. The compressive stress at a strain rate of 10-1 s^{-1} can be more than 0.4 MPa for hard hail, while the compressive stress at a strain rate of 10-1 s^{-1} can be less than 0.35 MPa for soft hail.

Tippmann (2011) obtained the results from the FE peak compressive force rather than the compressive stress due to the limitations of universal testing equipment. However, the compressive strength of artificial hailstones has a negligible influence on the maximum dent depth on steel sheet from the perspective of energy conservation.

Because of air bubbles trapped in opaque layers, hailstones have a lower density than pure ice (Brimelow et al., 2002; Crenshaw and Koontz, 2002; Engelbert, 1997). Hailstones have an average density of 910 kg/m^3 (Brimelow et al., 2002; Crenshaw and Koontz, 2002).

3.2. Hail Formation

Cumulonimbus clouds are formed from the contents of cumulus clouds. Cumulonimbus clouds, which are steep clouds, form hail. Hailstones, storms and electric charges (lightning) are contained in these clouds. As a result, these clouds pose a threat to air platforms. Due to the vertical shapes of these clouds, there is a temperature difference between the top and bottom of the clouds. A sudden change in temperature and an abrupt change in air flow result in hail formation. An explanation of the formation of hailstones has been provided by Wu (2018), who explained that hailstones originate from snow pellets, ice crystals, water drops and even dirt particles. According to Laurie (1960), hailstone formation begins when water vapour holds onto dust, salt, or other particles. Embryos are this particulate. Layer by layer, the particle freezes. In this case, the particle moves from the top of the cloud to the bottom of the cloud and holds onto each other. This circulation is responsible for the particle moving upward. A layer of clear and opaque hailstones may form when small hailstones are transported to another temperature zone. Layered structures suggest two types of growth. There are two types of growth: dry growth and wet growth. Figure 4 illustrates the formation of hailstones. A summary of the formation was provided.

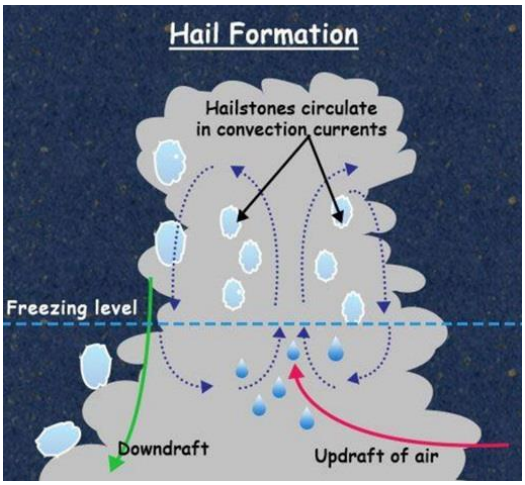

Figure 4. Scheme of the hail formation (Yilmaz et al., 2020)

As a result of dry growth, hailstones are carried to high altitudes where the air temperature is below zero degrees Celsius. The water droplets attached to the embryo immediately freeze within the cloud. As a result, the air is trapped inside and forms an opaque layer. When the clouds are wet, the air temperature is close to zero degrees Celsius, while the water content in the air is relatively high. It is believed that the water droplets that adhere to the hailstones do not freeze immediately during wet growth, but freeze slowly and expel all impurities and air, leaving a clear layer on the outside.

3.3. Methods of Making Artificial Hailstone:

It is possible to simulate natural hailstones using a variety of materials and methods. Based on the methods, there are some typical properties of natural hailstone, which are summarised in Table 1.

Table 1. The characteristics of natural hailstones and their comparison with artificial hailstones under different methods

Methods	Density	Crystal structure	Integrity	Onion-layered structure
Steel balls	X	X	OK	X
Pure ice hail	OK	X	X	X
Cotton ice hail	OK	X	N.A.	X
PVA hail	OK	X	OK	X
Liquid nitrogen hail	OK	OK	OK	OK
Natural hailstone	OK	OK	OK	OK

So far, various techniques have been used to simulate natural hailstones. However, most of these methods have failed to demonstrate the properties of the natural hailstone.

It has already been mentioned that steel balls or other penetrators have been used in impact tests, but this is only a demonstration of the integrity of the natural hailstone. Another popular method of simulating hailstones is to use artificial hailstones and demineralised water. However, in this method, the ice does not have the natural properties of the hailstone, i.e. it remains intact after being hit by an object. After impact, this artificial hailstone was broken. Figure 5b shows a hailstone made of demineralised water. The use of PVA glue increased the tensile strength of the ice.

After experimenting with different percentages of PVA and demineralised water, the author found that 12% PVA and 88% demineralised water were more successful in the impact tests. The intactness rate of the artificial hailstone made of demineralised water was higher than that of the artificial hailstone. Consequently, these methods did not simulate natural artificial hailstones. Figure 5a shows the section of an artificial hailstone to which PVA was added. Table 1 shows that natural hailstone can now be successfully simulated by using liquid nitrogen to produce artificial hailstone. Yilmaz et al. (2020) describe the use of liquid nitrogen to produce artificial hailstone. The latter two methods are used in this work to produce artificial hailstones. These artificial hailstones were then used in impact tests.

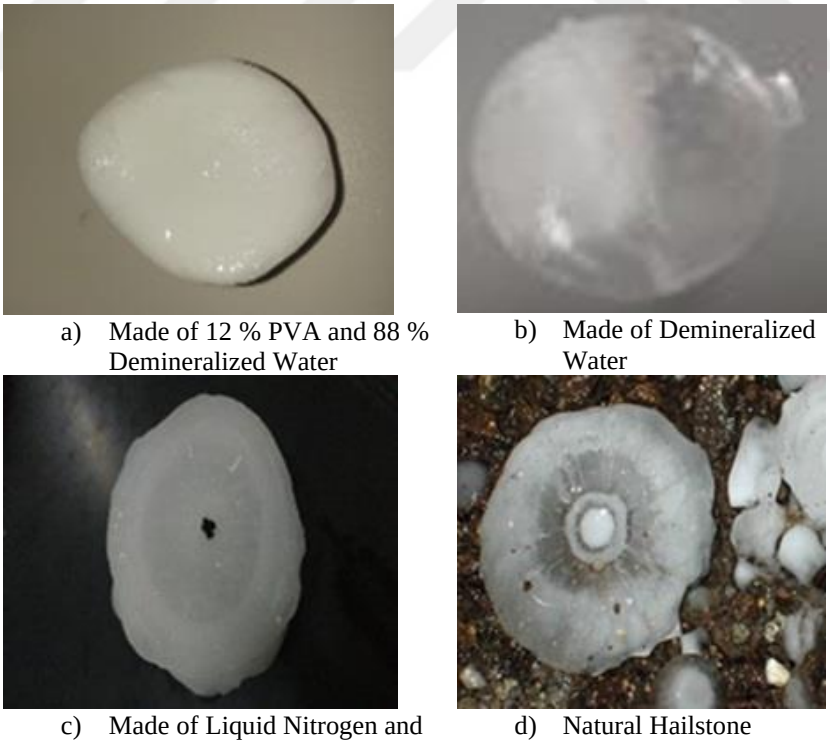

a) Made of 12 % PVA and 88 % Demineralized Water

b) Made of Demineralized Water

c) Made of Liquid Nitrogen and Demineralized Water

d) Natural Hailstone

Figure 5. The cross section of natural hailstones and artificial hailstones made by three different methods

In Figure 6b the artificial hailstone was made from cotton to test its breaking strength. However, in this method, the artificial hailstones have a higher breaking strength than the natural hailstones. The hailstone damages the target in a different way than the natural hailstone.

(a) Hail by Pure Water

(b) Hail by Cotton and Pure Water

(c) Hail by 12% PVA and 88% Pure Water

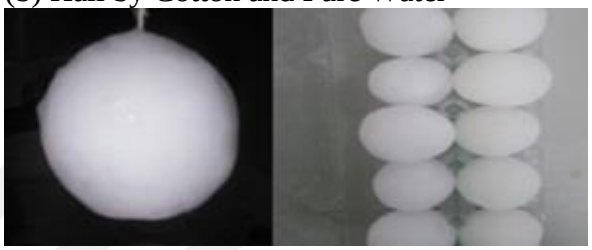

(d) Hail by Nitrogen Gas

Figure 6. Artificial hailstones of 45 mm diameter made using four different methods

3.3.1. Artificial Hailstones Based On 12 % PVA and 88 % Demineralized Water

Researchers have tried different combinations of PVA and demineralized water to produce artificial hailstones. Uz et al. (2017) have shown in Table 2 the intact situations of different percentages of PVA, demineralized water, and micro fiber which are used to make artificial hailstones.

Table 2. Artificial hailstone rates based on different methods (Bircan et al., 2018)

Impact Outcome	**5% PVA with 1% microfiber**	**11% PVA**	**12% PVA**
Intact	1	5	7
Minor Fragmentation	5	1	0
Broken	4	3	0

In the impact tests, the combination of 12% PVA and 88% demineralised water showed superior results. In this study, demineralised water supplied by Adnan Menderes University Laboratories was investigated. The materials used for the production of artificial hailstones are shown in Figure 7.

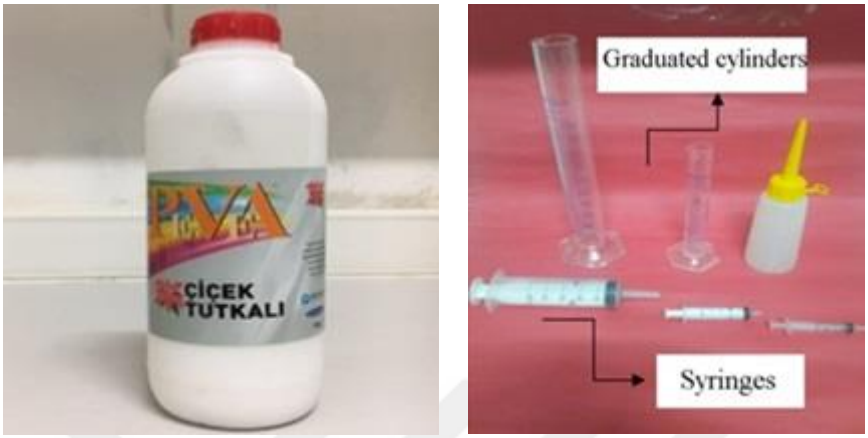

Figure 7. Materials used for artificial hailstones

The procedure for making artificial hailstone using 12% PVA and 88% Demineralized water is as follows:

1) Firstly, demineralized water should be boiled twice to expel the air and speed up the dissolution process

2) Using a graduated cylinder, enough PVA is added to the mixing bowl

3) Following the addition of PVA, enough demineralized water should be added to the mixing bowl

4) Stir the mixture for 15-20 minutes until it has completely dissolved

5) By using the syringe, fill the mold shown in Figure 8 with the mixture

6) Place the mold in the freezer with care

7) After 48 hours, remove the artificial hailstone from the mould and place it in the refrigerator to dry. If the mould sticks together, leave it at room temperature for a few minutes before attempting to remove the artificial hailstone.

8) Rub your finger along the mold's inlet hole to smooth out any air bubbles that may have formed.

This artificial hailstone will be used in the impact test after these steps have been completed.

Figure 8. Artificial hailstone molds

Artificial hailstones were made using 45 mm, 38 mm, and 50 mm molds. However, other diameters of molds are available in the laboratory.

3.4. Making Artificial Hailstone Using Liquid Nitrogen

Artificial hailstones have not been produced or simulated in the literature. Various methods and materials have been used for simulation, but none of them has been able to reproduce the full behaviour of natural hailstones. Hailstones form naturally in vertical cumulonimbus clouds. In the cumulonimbus cloud there is a temperature difference between the rising and downdrawn portions. To simulate artificial hailstones in laboratories, various methods have been used in previous studies. However, these methods are not sufficient to identify the characteristics of natural hailstones, as shown in Table 1. Therefore, Yilmaz et al. (2020) developed a new technique to produce artificial hailstones.

It is necessary to use two materials in order to create a natural hailstone formation environment. The first is cold material (at least -40 degrees Celsius). The other material is water with a temperature of +0 degrees. In the case of the cold material, liquid nitrogen was predicted and simulated. Laurie (1960) explained that hailstones contain an embryonic core.

A cross-section of a natural hailstone and an artificial hailstone made of liquid nitrogen and demineralised water is shown in Figure 9. As dust, salt and other particles are trapped by the water vapour, hailstones form. To simulate the embryo in this method, a knot is tied at the end of the nylon thread. The knot of the nylon thread is adapted to the embryo. Liquid nitrogen is used to simulate the top of the cumulonimbus cloud. The bottom of the cumulonimbus cloud consists of water with a temperature of 0 degrees Celsius.

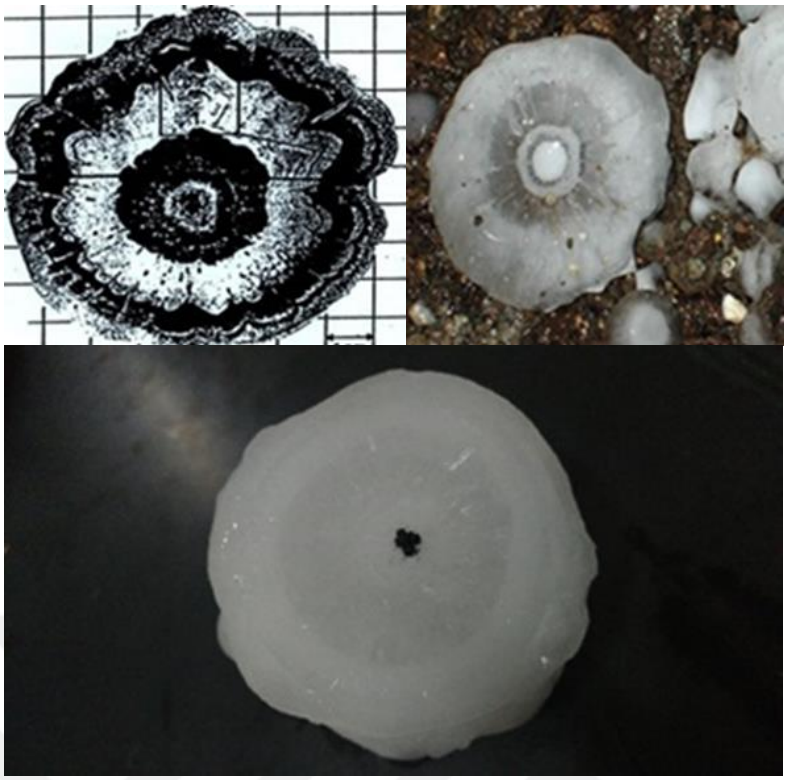

Figure 9. A cross-section of a liquid nitrogen hailstone and a natural hailstone

The materials used to make artificial hailstone using liquid nitrogen and demineralized water are described below and illustrated in Figure 10. Nitrogen in liquid form is represented by the chemical symbol "N". It is a non-metallic element. In nature, liquid nitrogen occurs as a diatomic molecule and, therefore, is symbolized as "N2" Density of liquid nitrogen is 0.808 grams per cubic centimeter. Boiling point of liquid nitrogen is -196 Celsius degrees. It has a melting point of -210 degrees Celsius. In general, distilled water consists of two hydrogen atoms and one oxygen atom. The mixture also contains calcium, magnesium, bicarbonate and other minerals. Distilled water is the removal of all these substances and minerals from water through various chemical processes. Generally, this water vapour is heated to 80 degrees Celsius and then condensed before being transferred to another container. The reason for using distilled water for artificial hailstones is that it is very similar to the water in clouds. The artificial hailstones were made with distilled water at a temperature of 4 degrees Celsius. Since rainwater contains other particles in the air, it cannot be used to make artificial hailstones. It was not necessary to use rainwater to make artificial hailstones with liquid nitrogen from the tap. The distilled water came very close to water when the water vapour condensed into water.

A liquid nitrogen tank is used to transform liquid nitrogen in a safe manner without harming the environment or evaporating. In the Dewar tank, the liquid nitrogen from the liquid nitrogen tank is converted into a form that allows the researcher to study comfortably.

The purpose of a pure water tank is to protect the contents of distilled water from spoiling without contaminating the contents. As a result of this condition experiment, the results will match the real situation. In a dewar vessel, water containers provide continuity for the liquid nitrogen immersion process. The core of the hailstone was simulated using a fishing line and an immersion mechanism. In the case of cuulonimbus clouds, this simulates the beginning of hailstone formation. The end of the fishing line should be immersed in distilled water. The immmerion mechanism produces more than one hailstone and facilitates the use of the device. Liquid nitrogen is used to make artificial hailstones in two containers. One is for pure water and the other is a dewar container. The end of the fishing line is tied with a knot to keep it in the water. In this way it is possible to simulate the natural hailstone embryo. The fishing line was first dipped in distilled water and then immersed in a Dewar container using this method. This process is repeated until the desired radius is achieved. Put distilled water (pure water) into a container that corresponds to the temperature in the cloud.

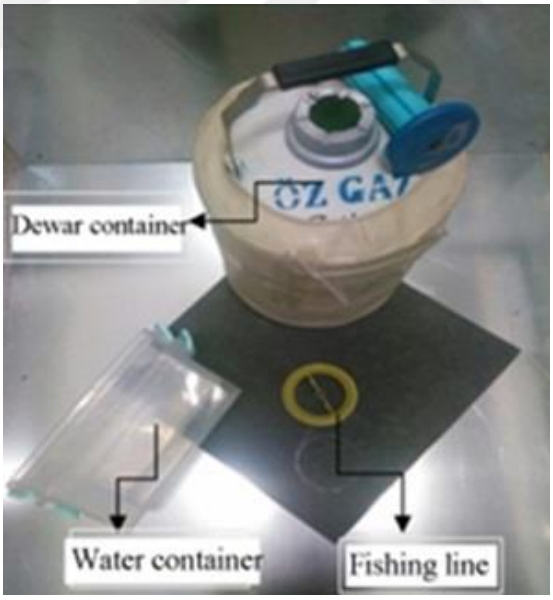

Figure 10. Liquid nitrogen and demineralized artificial hailstone materials

3.5. Standards for Hail Resistance

Tippmann (2011) explained the general standards of hailstone resistance. As a rule, the most common standards for hail resistance are as follows:

The artificial hailstone, which was made of liquid nitrogen and demineralized water, is not mentioned in these standards. Uz and Sizar (2021) compare other standards, as shown in Table 3.

Table 3. Comparison of Uz and Sizar (2021) and Standards for artificial hailstones

Standard	Artificial Hailstone	Diameter (mm)	Mass (gram)	Distance (mm)	Energy (Joule)
ASTM D-3746	Steel cylinder	50	2770	1355	22
FM 4473	Ice ball	31.8	15.3	<1500	5.5
		38.1	26.5	<1500	11.6
		44.6	42.1	<1500	20.9
		50.8	62.9	<1500	35.5
UL 2218	Steel ball	31.8	127	3700	4.6
		38.1	218	4600	9.8
		44.6	358	5200	18.3
		50.8	521	6100	31.2
Uz and Sizar (2021)	Demineralized water	45	44.9	1000	12
	Cotton and Demineralized water	45	45.1	1000	22
	12% PVA and 88 % Demineralized water	38	27.8	1000	10
		45	45.9	1000	19.9
		50	64.2	1000	32.0
	Liquid Nitrogen and Demineralized water	46	53.1	1000	22.7
		47	54.2	1000	22.8
		48	56.5	1000	23.4
		49	61.2	1000	25.3

It is possible to determine the impact resistance of bituminous roofing systems according to ASTM D-3746 (ASTM 2008). In 1996, Underwriters Laboratories published UL 2218, which covers impact resistance of prepared roof coverings (Underwriters Laboratories 1996). ASTM D-3746 (ASTM 2008) and UL 2218 (Underwriters Laboratories 1996) are focused on impact energy. Steel missiled and steel balls are used in the drop weight test. These drop from certain distance to reach to impact energy.

In accordance with FM 4473, rigid roofing materials are tested for their impact resistance by impacting them with a freezer ice ball (ANSI 2011). FM 4473 (ANSI 2011) uses ice balls for testing. Using a gas gun, ice balls are shot at designated speeds. Ice balls made of distilled water. At least 48 hours after freezing. There should be no air in ice balls. To projectile on the roof, ASTM-3746 uses a specific diameter object. In contrast to that standard, both FM 4473 and UL 2218 use four different diameter projectiles for testing. In all standards, if there is no visible dent or breakage caused by artificial hailstones, the device will pass the test. There are other specifications as well. AST:E 822-92 (ASTM 2009) is used to regulate hail damage to solar collector covers. The ASTM:E 1038-98 (ASTM 2004) is used to define photovoltaic modules based on the hail resistance. Hailstones are simulated using ice balls in these specifications. In aerospace engineering, ASTM:F320-10 (ASTM 2010) is used to assess hail damage, and cotton ice balls are used to simulate hailstones. Using liquid nitrogen and demineralized water, Uz and Sizar (2021) developed a standard for artificial hailstone. Artificial hailstone was made using three different methods.

4. EXPERIMENTAL ANALYSIS

In this study, after making artificial hailstones, the artificial hailstones were observed under experimental conditions. Uz et al. (2017) have created a laboratory for conducting impact tests at the Aydın Adnan Menderes University. Uz et al. (2014) created these experimental setups in Australia as well. To increase the tensile strength of the artificial hailstone, experiments were conducted using demineralized water artificial hailstones prior to using PVA. In this thesis, artificial hailstones made of liquid nitrogen and demineralized water are analyzed, as well as artificial hailstones made of 12% PVA and 88% demineralized water. The experiments are based on a pneumatic dynamic impact test.

4.1. Dynamic Hail Impact Test

As with the previous studies presented in this thesis, experimental tests are conducted using the pneumatic dynamic impact test. The test setup consists primarily of the hail gun, protective unit, and measurement devices. Figure 5 illustrates the test setup. The density, volume and mass of the artificial hailstones are measured prior to the impact test. An air compressor is used in hail guns. To launch the projectile, pressurized air was provided by the air compressor. Figure 11 shows how the hail holder protects the hail from the damages caused by pressure.

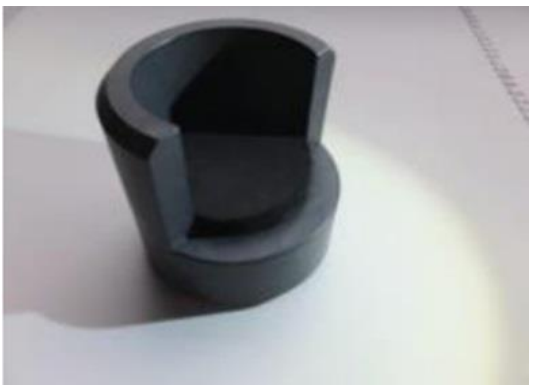

Figure 11. Hail holder (Maguire, 2014; Uz et al., 2014)

The hail cannon consisted of a regulator of pressure to calculate the pressure in the cannon, an air tank that collected the pressure and served as a release valve, a gas valve that acted as a trigger when the standard setting was closed, a movable mount that could be adjusted in height to shoot different projectiles, and finally a barrel to hold the hailstones.

There is a simple box-shaped structure to the protective unit. The design is shown in Figure 12. Its edges are made of iron square profiles and its walls are made of particle board. Figure 13 illustrates the cross section of the protective unit. The unit was designed to obtain a barrier between the experimental area and the outside environment. There is a mount that stabilizes the steel sheet at various angles. There is a large glass window on the impact protective unit that can be used for observing and recording. Two rows of five holes are included in the protective unit. Using these holes, it is possible to place the barrel inside the steel sheet and shoot at different parts of it. The velocity sensors are also mounted on a rail. The unit had a door on one side.

Figure 12. Protective unit design (Maguire, 2014; Uz et al., 2014)

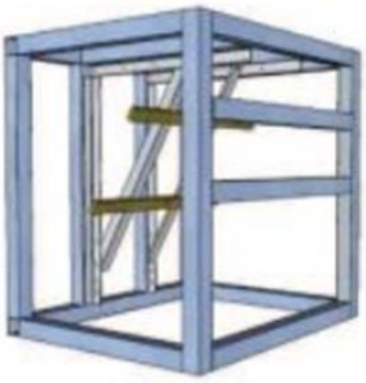

Figure 13. Steel frames of protective unit (Maguire, 2014; Uz et al., 2014)

On one side of the protective unit, a high-speed camera records hailstone impacts and measures their speed (see Figure 14b).

A 185-watt LED light connected to a DC converter was acquired to supply sufficient lighting for a high-speed camera to operate without flickering in video footage with high frame rates.

By trial and error, the frame rate of the camera was set to 1000 frames per second to accurately measure the flight distance of artificial hailstones. To avoid a darker image due to a higher frame rate, three powerful DC lights were used, two outside and one inside the unit. Figure 14a illustrates an air compressor and a hail gun. Hail guns are equipped with hail holders.

A whiteboard scale can be used to determine the launch velocity of artificial hailstones as shown in Figure 15. The impact velocity of the artificial hail was calculated using the number of images taken by the camera and the distance from the scale.

a) 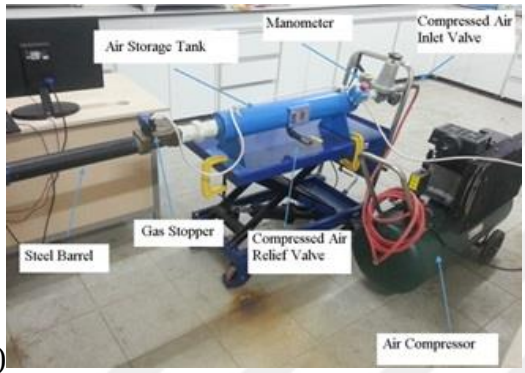

b) 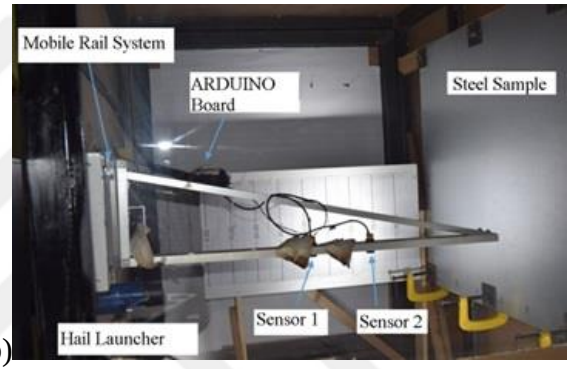

Figure 14. Test equipments

Additionally, the high-speed camera provided the opportunity to examine artificial hailstones during impact. To validate the speed detected by the high-speed camera, the speed sensors were mounted on the mounting frame and connected to an Arduino board using MATLAB, as shown in Figure 14. Two laser sensors were used for the dynamic impact tests. They were connected to an Arduino logic board via a rail system inside the protection unit. One laser sensor is placed after another so that the artificial hailstone can be detected. An Arduino board was programmed to output the time between detections by the first and second sensors.

The speed is measured by the time taken by the lasers and the distance between the two lasers is known. Since the test setup has two rows of launch apertures, the sensors are rotated upwards when using the top row and downwards when using the bottom row. As can be seen in Figure 14 and Figure 15, the measurement setup for velocity can be seen. The steel sheets are then subjected to hailstone impacts. The steel sheets change after ten shots.

a)  b) 

Figure 15. Images of a 38 mm diameter PVA hailstone fired at 43.5 psi: a) before impact, b) after impact with the steel plate

After the impact experiments, the hail launcher was depressurised. After the pressure in the hail thrower has been released, the depth and diameter of the dent are measured on a steel sample. The diameter of the dent and the depth of the dent were measured with the greatest possible accuracy. The measurements are carried out according to Figure 16. The dent depth and the diameter of the dent in the 0.3 mm thick steel sheet are shown in Figure 16. A digital calliper was used to measure the diameter of the dent. A depth calliper was used to measure the depth of the dent. Due to the scope of the current study, the configuration and angle of the steel plates are not considered in this study.

4.1.1. Measuring Dent Depth

The measurements of the dent depth and the dent diameter are also important for the study. Each steel sheet was shot ten times. After the ten shots, the steel sheet was changed. The shape of hailstones is spherical, but the shape of the dent caused by the impact is not spherical. Since the shape of the dent is not perfectly spherical, three axes are defined, and the diameter of the dent is measured from three different axes and recorded on the result sheet. The average of these three values was used to determine the diameter of the dent. The diameter of the dent was measured with a digital calliper.

Figure 16. Measurement of dent depth and diameter in 0.3 mm steel panels

The depth of the dent was measured after the diameter of the dent was measured. There is a difference in depth in the impact area due to the impact. The maximum depth of the dent was measured and recorded. Due to equipment limitations, the depth and diameter of the dents are measured with a gauge. There were two ways for measuring depth and diameter of the dent. Wu (2018) used a 3D scanner. However, only gauge measurements are available in the current study.

5. ANALYTICAL ANALYSIS

For various sectors it is important to be able to predict the damage caused by hailstones. This is especially true for the automotive industry. As the impact of hailstorms on cars and roofing will increase in the future, hail days will increase. Consequently, predicting the depth of the dent will become even more important in the future. Various researchers have so far tried to establish an equation for predicting the dent depth. However, there is no work in the literature that deals with the calculation of damage considering the yield stress of the material and the thickness of the sheet. Meanwhile, Uz et al. (2021) presented an equation to predict dent depth based on material properties such as yield stress and sheet thickness. In this study, an equation function of kinetic energy and sheet thickness is proposed. The energy conversation can be written as Eq. 1 to determine the damage caused by collisions.

$$E_{Impact} = E_{Vibration} + E_{Plastic} + E_{Rebound} \quad (1)$$

Vibration energy ($E_{vibration}$), which converges to zero, is an important component of impact energy while rebounded energy converges to zero ($E_{Rebound} \cong 0$). The yield stress of a material and its volume change determine the plastic energy ($E_{Plastic}$) during impact. The thickness of the material approaches zero during impact; therefore, the plastic energy can be calculated using Eq. 2.

$$E_{Plastic} = \sigma_y t \Delta A \quad (2)$$

As shown in Eq. 2, the thickness of the steel sheet demonstrated by t and σ_y represents the yield stress of the impacted steel sheet. Eq. 3 explains how to calculate the change in area. It is possible to determine the change in area (ΔA) by comparing the distance between the datum area and the deformed area after the impact. In Figure 17, a cross-section of a partly spherical dent is shown. Based on Eqs.5-7 and Figure 17b, a diagram of the stress-strain behavior during denting is shown in the bachelor thesis of Maguire (2014), for which the first author of the present study was a co-supervisor.

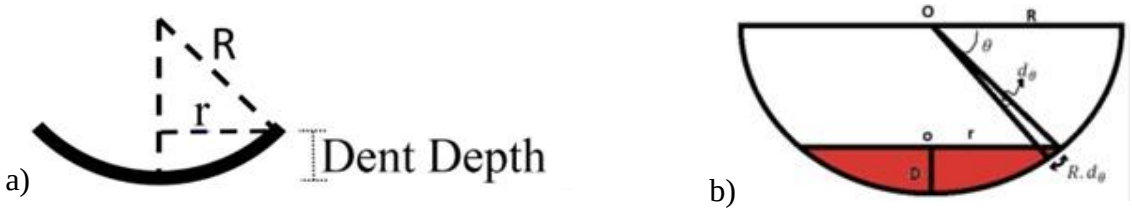

Figure 17. Cross-section of a) dent shape and b) dent area

A simplified dented area is symbolized by before the collision by r. Additionally, R indicates the radius of the artificial hailstone. Dent depth is denoted by D. As a result of the geometry in Figure 17b, the initial (original) dent area can be calculated as follows:

$$\Delta A = A_f - A_0 \quad (3)$$

$$A_0 = \pi r^2 = \pi(R^2 - (R - D)^2) = \pi(2RD - D^2) \quad (4)$$

In Eq. 5, the area deformed because of the impact is given. The change in area and the plastic energy can be calculated using Eqs. 6 and 7.

$$A_f = \int_{\theta}^{\frac{\pi}{2}} 2\pi r R d_\theta = 2\pi RD \quad (5)$$

$$\Delta A = \pi D^2 \quad (6)$$

$$E_{Plastic} = \pi D^2 \sigma_y t \quad (7)$$

The oscillation energy shown in Eq. 1 is called spring energy in the theory of conservation of energy. With the aim of developing a realistic equation, a simplifying assumption is made in this thesis. Although the spring is compressed by the impact force for a short period of time, the spring does not produce the effect of momentum loading because it is difficult to measure the time interval during impact in an experimental study. In addition, the impact is almost instantaneous due to the external vibration generated by the hailstone impact and the external frequency of the hailstone is assumed to be zero. If the system is stable under this assumption, Eq. 8 can be used to express the pressure distance under sinusoidal steady state behaviour.

$$x = u_{st}\left|H_{jw}\right| \cos(\omega t + F) \quad (8)$$

When $\omega = 0$,

$$\left|H_{jw}\right| = \sqrt{\frac{1}{(1-\left(\frac{\omega}{\omega_n}\right))^2 + (2\delta\left(\frac{\omega}{\omega_n}\right))^2}} = 1$$

$$\tan(F) = \frac{2\delta(\frac{\omega}{\omega_n})}{1-(\frac{\omega}{\omega_n})^2} = 0 \quad \rightarrow \quad F^o = 0^o$$

$$\left|H_{jw}\right| \cos(\omega t + F) \cong 1 \quad (9)$$

In Eq. 9, $\left|H_{jw}\right|$ is shows that the dynamic amplification. It means that the vibration energy is equal to:

$$E_{Vibration} = \frac{k}{2} \cdot \frac{F^2}{k^2} = \frac{F^2}{2k} \quad (10)$$

In the Eq. 11 it was shown that the flexural stiffness (k) of a flat plate is proportional to the thickness of the steel (t) and the third power of the length of the plate (h), but inversely proportional to the third power of the distance between the battens.

$$k = \frac{Eth^3}{l^3} \quad (11)$$

A study was performed in which E, and h defined the elastic modulus of the sheet and the transversal length (l) of the sheet plate is the distance between the center of the dent shape and the closest timber batten screwed to the flat steel sheet. To cause a dent on the target, a force must be generated between the material's elastic behavior limits, as determined by the stress-strain curve. When the yield stress point is reached on a flat steel sheet, the spring of the material is compressed by the force found with $F = \sigma_y A$. The assumption was made that the compressive area converged to the cross-sectional area of the hailstone. A hailstone's diameter (2R) is represented by the symbol φ in the following equation. The force applied to the flat sheet as a result of hailstone impact is rewritten. To clarify the vibration energy, Eq. 12 can be now inserted into Eq. 10. Therefore, the vibration energy is equal to

$$F = \sqrt{\frac{{\sigma_y}^2 \pi^2 \varphi^4}{16}} \quad (12)$$

$$E_{Vibration} = \frac{{\sigma_y}^2 \pi^2 \varphi^4 l^3}{32Eth^3} \quad (13)$$

Finally, the energy conservation Eq. 1 is now rewritten to obtain the dent depth:

$$D = \sqrt{\frac{mV^2}{2t\pi\sigma_y} - \frac{\sigma_y \pi \varphi^4 l^3}{32Et^2h^3}} \quad (14)$$

It is possible to optimize and revise the dent depth in Eq. 14 by considering the rebounded energy and the compressive area by using the following formula:

$$D = \sqrt{\alpha \times \frac{mV^2}{2t\pi\sigma_y} - \beta \times \frac{\sigma_y \pi \varphi^4 l^3}{32Et^2h^3}} \quad (15)$$

where α and β are the coefficients for rebounded energy and compressive area, respectively. As a result of an impact, energy is dissipated by a factor known as the Coefficient of Restitution (COR). An elastic event occurs when COR is equal to unity. When the surface deformation of the contacting objects falls within the elastic range, this event is unusual (in terms of material behavior). Therefore, the impact is not elastic but partially plastic.

When COR = 0, a perfectly plastic impact is assumed. The most common definition of COR is the ratio between the final relative velocities and the initial relative velocities of the two objects. According to the current study, COR is calculated as follows:

$$COR = \frac{\text{Rebound Velocity}}{\text{Impact Velocity}} \quad (16)$$

It is possible to identify a broken or smashed hailstone (COR = 0) during impact by obtaining, α in Eq. 15 is obtained as

$$\alpha = (1 - COR)^2 \quad (17)$$

Since a digital 3D scanner was not available in the present experimental study, it was difficult to measure the exact value of the dent diameter (D_d) by using a depth gauge manually after impact.

Figure 18 illustrates the cross-section of the measured compressive dent diameter after impact. To determine the effective stress when the steel plate deforms in the elastic region, the author focuses on the compressive area in Eq. 13.

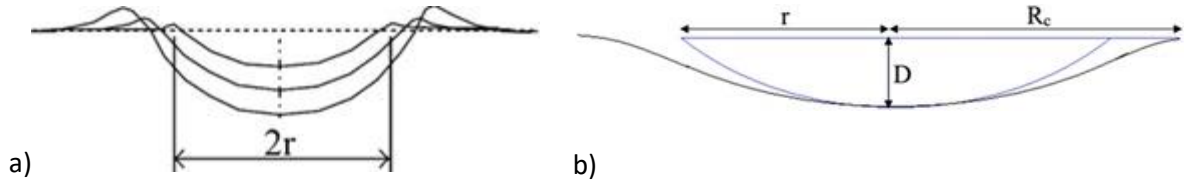

Figure 18. Observed dent shapes during elastic behavior of steel plates: a) compressive strains during impact, b) observed compressive strains during impact

Figure 18b illustrates the observed dent profile. The coefficient of $\beta = \frac{2R_c}{\varphi}$ is determined by the compressive area. The β coefficient can be calculated in according to the distribution of the steel plate thickness and hailstone diameter parameters given in Table 4. A steel plate's compressive radius is defined as R_c in elastic behavior, while an elliptic dent radius is defined as r.

Table 4. The β coefficient values based on hail diameter and panel thickness

Sheet thickness (mm)	Hailstone diameters (mm)		
	50	45	38
0.3	0.28	0.32	0.37
0.45	0.34	0.38	0.43
0.6	0.4	0.44	0.49
0.7	0.46	0.5	0.56
0.8	0.51	0.55	0.6
1.0	0.56	0.6	0.65

The change in area (ΔA) after collision is redefined by the Knud Thomsen formula to calculate an approximation of the surface area of an ellipsoid using the lengths of the semiaxes as given in Figure 18b. According to this determination, the planar area before the impact is unchanged ($A_0 = \pi\,(2RD - D^2)$), while the deformed area (A_f) is similar to the surface area of an oblate spheroid defined according to Knud Thomsen's surface area formula as follows:

$$A_f = 4\pi\left(\frac{(ab)^p + (ac)^p + (bc)^p}{3}\right)^{\frac{1}{p}} \qquad 18$$

For $p = 1.6075$, $a = b = r$ and $c = D$. In this situtation (half ellipsoid), the elliptic dented radius (r) is determined as $r = \sqrt{R^2 - (R - D)^2}$, where R and D are the radius of the artificial hailstone and the dent depth, respectively. Therefore, the equation is equal to:

$$A_f = 2\pi\left(\frac{r^{3.215} + 2(rD)^{1.6075}}{3}\right)^{1/1.6075} \quad 19$$

And the revised changed area after collision is:

$$\Delta A_r = A_f - A_0 \quad 20$$

$$\Delta A_r = 2\pi\left(\frac{r^{3.215} + 2(rD)^{1.6075}}{3}\right)^{1/1.6075} - \pi r^2 \quad 21$$

Therefore, $\varkappa = \frac{\Delta A_r}{\Delta A_i}$ and $\Delta A_i = \pi D^2$. Finally, the revised plastic energy equation is equal to:

$$E_P = \varkappa \pi D^2 \sigma_Y t \quad 22$$

And the proposed dent depth equation is rewritten as:

$$D = \sqrt{\frac{\alpha}{\varkappa} \times \frac{mV^2}{2t\pi\sigma_y} - \frac{\beta}{\varkappa} \times \frac{\sigma_y \pi \phi^4 l^3}{32Et^2h^3}} \quad 23$$

A constant yield stress (σ_y), Young's modulus (E), average effective length (l), and transversal length (h) are maintained in laboratory conditions ($\sigma_y = 320$ MPa, E = 200 GPa, l = 148.7 mm, h = 1 m). The $\varkappa$ coefficient is determined by the ratio between the radius of the artificial hailstone and the elliptic radius of the dented area as shown below. Therefore, when the ratio of the radiuses increases, the $\varkappa$ coefficient determined by the ratio of ΔA_r and ΔA_i increases proportionately. The $\varkappa$ coefficient is shown in Figure 19. The remaining kinetic energy is converted into plastic energy when the steel material reaches the yield stress. Therefore, Work that is applied along the depth direction will be equal to the plastic energy as well as work that is applied outside the dent ellipse shown in Figure 18b is in a negligible level. The relationship between R_c and r is found from the experimental tests to be $r = 0.58R_c$, with 0.2 mm tolerance.

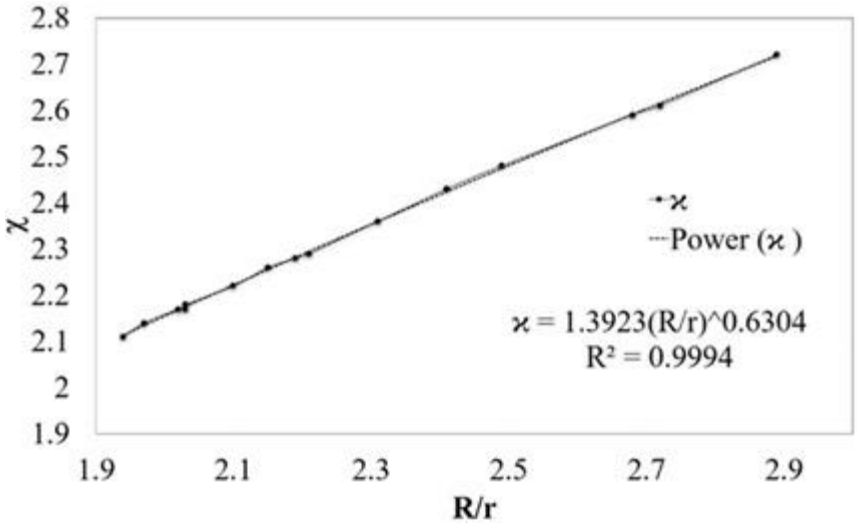

Figure 19. Values of the $\varkappa$ coefficient with the ratio of R/r

Based on the relationship between the $\varkappa$ coefficient and the radius of the artificial hailstone compared to the radius of the elliptical dented shape, the $\varkappa$ formula is shown below:

$$\varkappa = 1.3923(\frac{R}{r})^{0.6304} \qquad 24$$

For a particular impact energy, Johnson and Schaffnit (1973) suggested that the dent depth is inversely proportional to the square of the sheet thickness. According to Wu (2018), the dent depth is inversely related to the square roots of the sheet thickness and the yield stress. Eq. 23 can be used to calculate the dent depth by combining the plastic energy with the rebounding energy and vibration energy with the compressive area.

6. FINITE ELEMENT ANALYSIS

A description of the current finite element model and previous numerical studies about hailstones is provided in this section of the thesis. Using finite element analysis, researchers can simulate hailstones on a computer and validate experimental and analytical results. ABAQUS 2020 was used for the analysis of infinite elements in this thesis.

6.1. Previous Finite Element Models for Hailstone

In the previous section of the thesis, it was mentioned that hailstone has a complex structure. It is difficult to simulate and model FE analysis related to it. However, researchers have attempted to model the material of hailstones. The following section presents finite element models.

6.1.1. Material Model by Kim and Kedward

Kim and Kedward (2000) developed a material model using LS-DYNA3D (Lawrence Livermore National Laboratory Version). The results of this study were compared between monolithic and flat-wise layered ice experiments. In this study monolithic and flat-wise layered ice experimental results were compared. Figure 20 illustrates the monolithic and flat-wise layered ice used by Kim et al. (2000). In this study, DYNA3D was used for the material model of the type 13 elastic-plastic with failure. To set the shear stress components in failed elements to zero, the failure strain and failure tensile pressure criteria were applied to the model with only hydrostatic compressive stresses (i.e. fluid-like). Although the same material model parameter values were used for all cases of SHI diameter and velocity, the strain rate was not considered. The material parameter values were obtained by comparing the experimental results with the simulation results. Although the overall shape of the force curve generally matched well, the peak value of the force differed significantly.

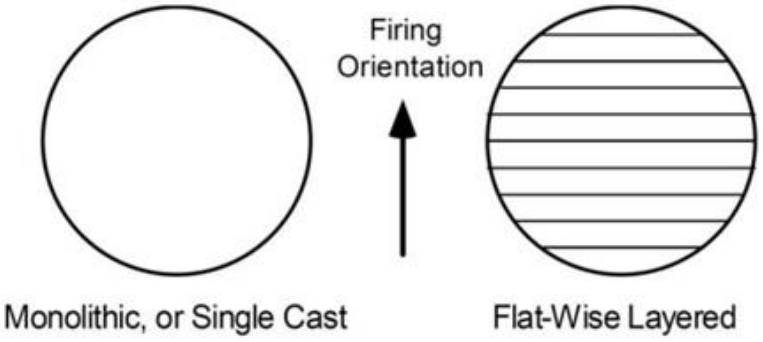

Figure 20. Two different structures of ice

6.1.2. LS-DYNA Model by Kuene

The material model of Kim and Kedward (2000) was developed by Kuene (2004). Kuene (2004) used the same elastic-plastic with failure type material in LS-DYNA. The material inputs for each test condition differ, particularly the yield strength and failure pressure. As a result of the development of a relationship, it is possible to select appropriate values based on the size and velocity of the projectile. In comparison with Kim and Kedward (2000), the simulation results showed a much closer match with all the experimental data.

6.1.3. ABAQUS Model by Park and Kim

ABAQUS model developed by Park and Kim (2006) is similar to the model developed by Kuene (2004). A similar set of modifiable parameters, yield strength and tensile failure, was used in the ABAQUS model. Other parameters, such as element deletion and bulk viscosity, were developed by Park and Kim (2006). The researchers compared the force histories with the results of the previous model.

6.1.4. Ice Material Model with Strain Rate Dependent LS-DYNA by Carney et al.

Carney et al. (2006) aimed to determine the threshold for critical damage to the Space Shuttle orbiter's leading edge due to ice impacts. Researchers developed a phenomenological high strain rate ice material model using LS-DYNA. According to Carney et al. (2006), the material model consisted of independent compression and tension failure levels, as well as strain rate-dependent failure parameters. In contrast to previous studies, this study utilizes LS-DYNA's multi-material Eulerian capability in which the projectile is represented as a Eulerian mesh domain and the target as a Lagrangian domain. In this study, the cylinder impact force history measurements were compared with the material model.

6.1.5. Material Model by Tippmann

Tippmann (2011) examined the properties of hail materials. Finite element analysis of hailstone was performed using Abaqus. A combination of experimental and finite element analysis is used in the study of Tippmann (2011). Experimental and finite element approaches were compared in terms of impact forces. Additionally, Tippmann (2011) validated the results of previous studies and used used three different diameters of hailstones. The diameters of these hails are 61 mm, 50.8 mm, and 38.1 mm, respectively. The mesh was constructed using a Lagrangian domain mesh.

6.2. Validation of Previous Studies

To simulate the hail impact on the flat steel plate, Abaqus Explicit was used. The main purpose of the finite element model is to validate the dent depth and diameter determined experimentally and analytically in this study. Therefore, the finite element model was developed in this work. The validation of FE models is primarily determined by experimental results. To obtain a successful finite element model, it is necessary to collect the appropriate field data for material properties, boundary conditions and contact algorithms to successfully run the FE models. To achieve this goal, validations are performed with the experimental and finite element results obtained by other researchers. As shown in Eq. 25, the smallest element in the model affects the stable time increment in Abaqus/Explicit. Therefore, uniform elements in the model are desirable for faster calculation.

$$\Delta t = L_e/\sqrt{E/\rho} \qquad \textbf{25}$$

where L_e is the length of the smallest element. E and ρ are the modulus of elasticity and density, respectively. For the mesh, the traditional Lagrangian mesh was chosen. For the hail and plates, the mesh type in Abaqus/Explicit was chosen as C3D8R linear elements with reduced integration. In the current study, different mesh sizes were used for validation as shown in Figure 21. After investigation, better agreement was found for each test. Figure 22 shows that the finite brick element (C3D8R) is meshed on the artificial haistone. Due to the symmetry, all validation hails and the slab could be modelled as one quarter to reduce cost and computation time. On the other hand, scale models are used in the validations to avoid distortions and instability problems due to the impact, as shown in Figure 23.

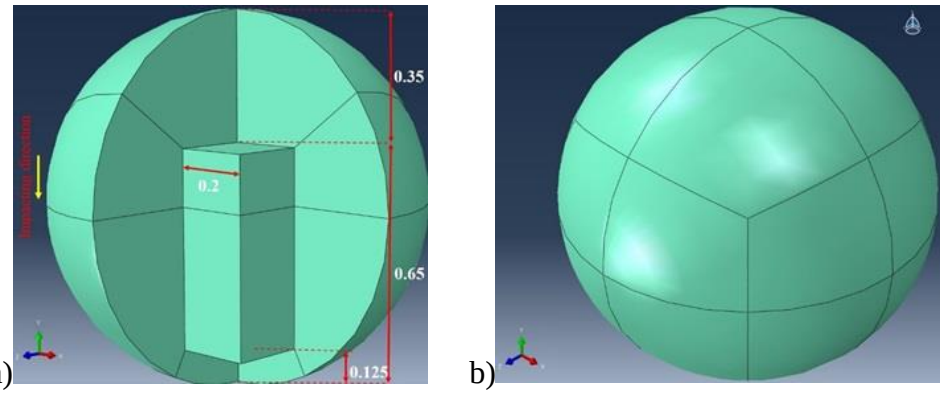

Figure 21. a) Sketch of key sphere dimensions with normalized unit diameter b) Fully partitioned hailstone model by Uz et al. (2022)

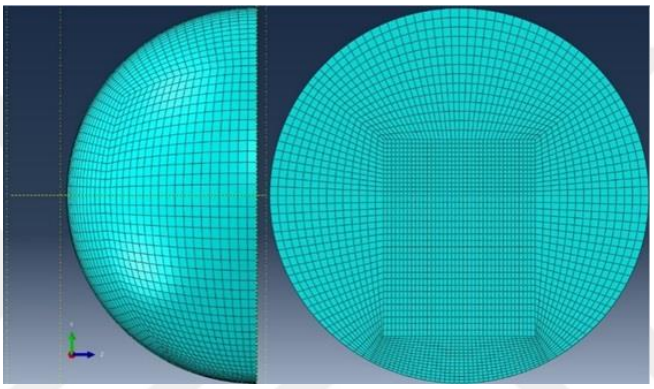

Figure 22. Finite brick element (C3D8R) mesh

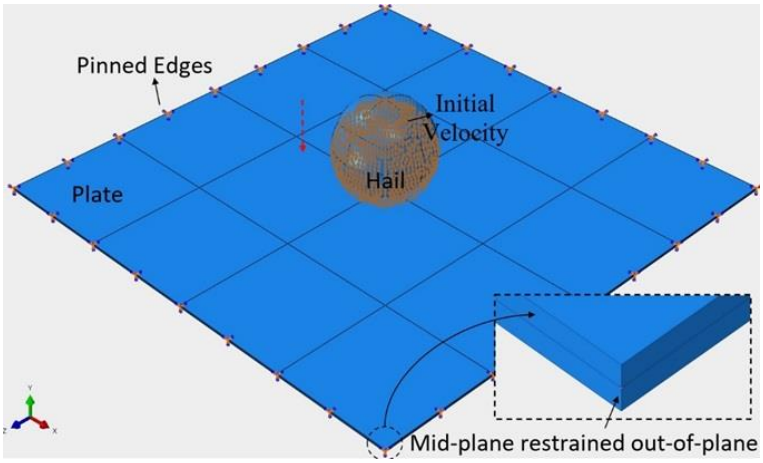

Figure 23. Conceptual model

Figure 24 shows an example of the mesh of a full-size validation model. The impact of a hailstone with a diameter of 50.8 mm on a steel plate of 200 x 200 mm^2 is shown. To obtain the correct deflection of the plate, four elements are used across the entire thickness of the plate, as shown in Figure 24.

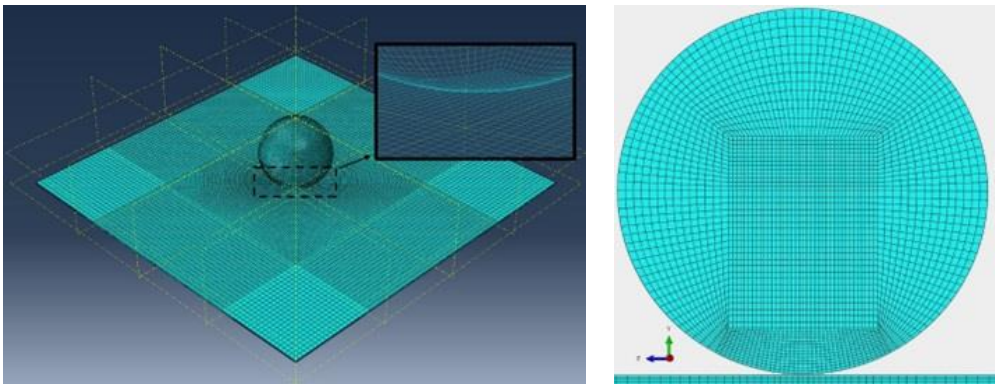

Figure 24. Full scale of 50.8 mm hailstone and 200x200 mm^2 flat steel sheet

On the plate, a bias of 4 was used to create 40 elements around the predefined field. The surfaces of the plate and the hail were used to determine the general contact with a hard and a punishing interaction property. The author chose Dynamic/Explicit as the impact level and added a period of 0.003 seconds predicted from the experiment as the average impact duration. The linear and quadratic bulk viscosity are assumed to be 1.2 and 0, respectively, in this study based on the sensitivity study by Park and Kim (2006).

6.2.1. Validation of Anghileri et al.

Anghileri et al. (2005) conducted an impact test with hail on a deformable plate of aluminium alloy with a size of $305 \times 305 \times 0.91$ mm. The edges of the plate were secured with blind rivets.

To simulate the real case of the structural performance of the plate for high-speed aircraft, a hailstone with a diameter of 25.4 mm was impacted on the target plate at a speed of 192 m/sec. This validation is important to ensure that the developed model will perform satisfactorily at high impact velocities. All details of the experimental test setup were modelled in Abaqus/Explicit according to the experience. Based on a Lagrangian FE model of the hailstone, an impact simulation is performed and the deflection of the plate along the profile length is calculated. According to Figure 25, the experimental result of the deflection profile in the study by Anghileri et al. (2005) was compared with the results obtained in this study using the model FE.

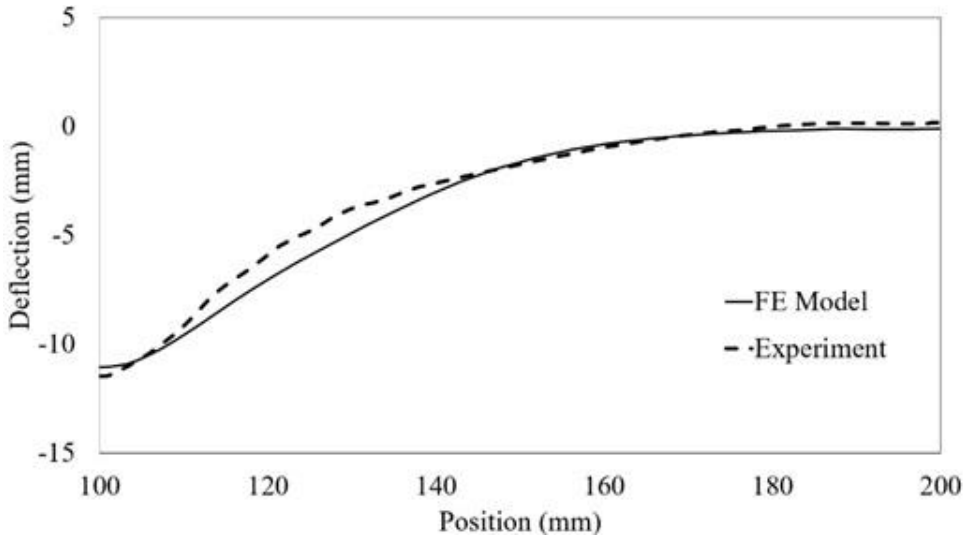

Figure 25. A comparison of hail impact deflection profiles at $\mathbf{t = 1.485 \times 10^{-4}}$ with Anghileri et al. (2005)

The trend of the deflection profile, as well as the maximum deflection at the center of the plate, are consistent with those obtained from the experiment. To confirm the hail fracture that can be observed after impact in the real case, Figure 26 shows the hail's deformed shape.

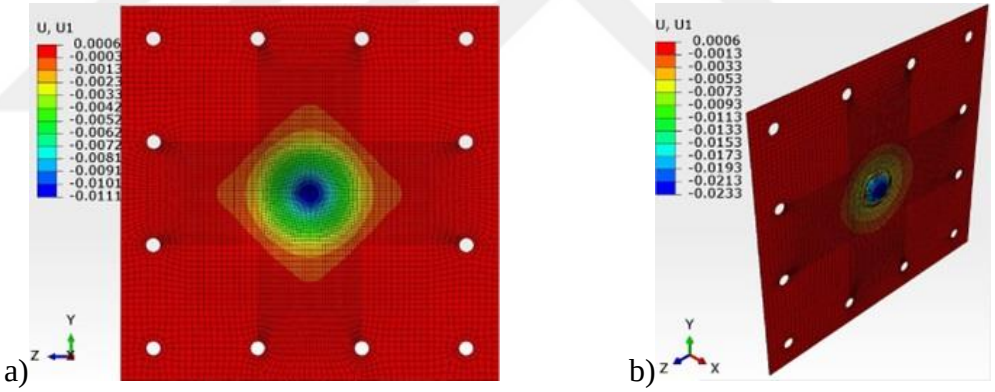

Figure 26. Displacement values of a) Plate b) Hailstone with fracture pattern

FE models are validated under high-speed hail impacts as well as different target plates such as aircraft, vehicles, and rigid panels.

6.2.2. Validation of Carney et al.

To validate the results of Carney et al. (2006), experimental results were used to investigate the behavior of ice during impact. For the projectile, cylindrical ice with a diameter of 17.5 mm and a length of 42.2 mm was used on a rigid plate. To measure the force time history for each test, a force transducer device was used behind the rigid plate.

Using 3D analytic rigid shells, the finite element model is set up with the same geometry and rigidity as the experimental test plate. In Figure 27, three discrete spring elements are used to fully fit the target plate to the test condition based on its modal characteristics. According to the finite element model, spring elements are described by following the line of action axis. The boundary condition of the FE models presented in this study allows the target plate to move only through the spring elements during impact. Impact force-time histories recorded by the force transducer device are compared with those extracted from FE models.

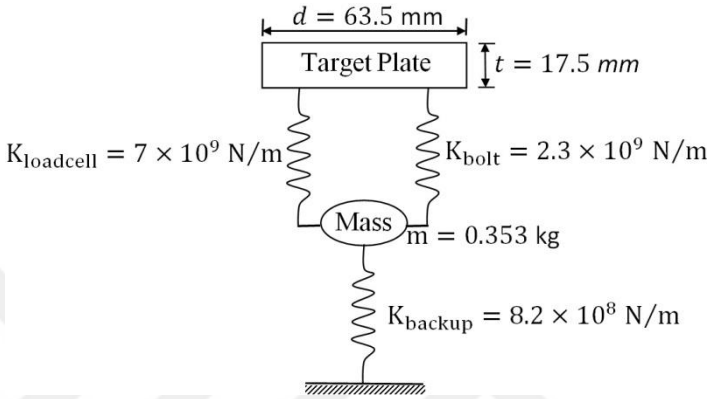

Figure 27. Schematic representation of the steel cylinder (load cell) and supporting springs

6.2.3. Validation of Tippmann

Tippmann (2011) examined the impact force on the plate. In that study, the Abaqus model was extended. The experimental and FE results were compared. A comparison is presented between the force time history from experiment test UCSD 195 conducted by Tippmann (2011) and the FEM generated by a 50.8 mm hail impact test conducted at 60.6 m/sec. In Figure 28, a comparison with Tippmann's (2011) experiment shows good agreement between the initial force pulse with large oscillations after 0.15 ms.

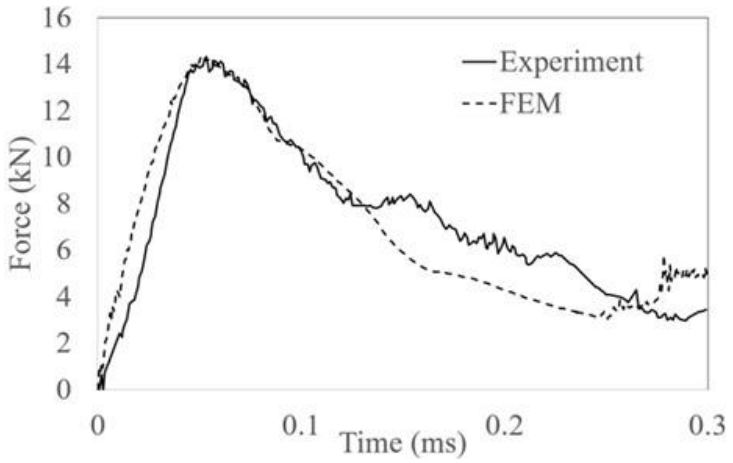

Figure 28. Comparing a finite element model (FEM) with an experimental test (UCSD 195) by Tippmann (2011)

6.2.4. Validation of Somasundaram

The purpose of study conducted by Somasundaram (2013) is to characterize hail impacts on vehicle body panels in terms of deformation size and shape as well as to consider FE modeling for hail impact. According to the results of the experimental study, hail impacting a bannet at around terminal velocity causes dent diameters between 9 mm and 28 mm and dent depths between 0.20 mm and 1.49 mm. Somasundaram (2013) found that dent diameters varied between plate sizes from 25.6 mm to 24.9 mm and dent depths varied from 1.79 mm to 1.59 mm with increasing plate size, which is up to 6.7% greater than the largest dent observed in the experiments (1.49 mm). The FEA results presented in Somasundaram (2013) indicate that dynamic effects, such as plate oscillations, were not considered. To obtain the final dent depth, dynamic effects must be dampened out. As a result, springback modelling is employed in the current study to validate the experiment results properly. It is necessary to use both explicit and implicit solvers when simulating springback models. With Abaqus, it is possible to change simulation between implicit and explicit solvers at user-defined time intervals using the initial state option under the predefined field option. Figure 29 illustrates the maximum deflection during impact. Using springback modeling, the final permanent deformation of the plate can be obtained as shown in Figure 30.

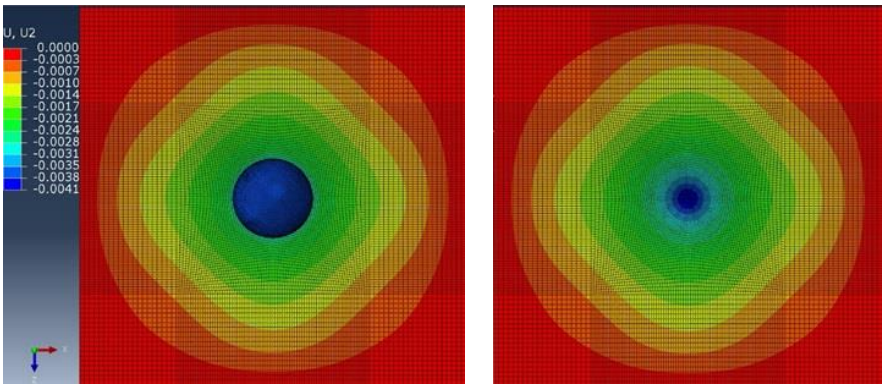

Figure 29. Simulation of a 40 mm hailstone impacting at 19.8 m/sec on 200 mm×200 mm flat sheet

To determine the depth of the dent, the average permanent deformation surrounding the contact diameter was subtracted from the permanent deformation at the center node. After damping out, the dent diameter and dent depth for the related plate size were calculated as 20 mm and 0.81 mm, respectively.

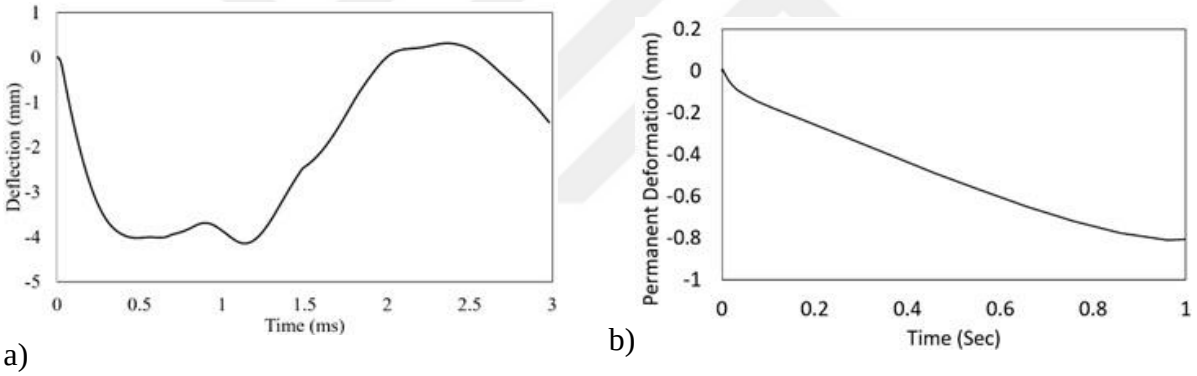

a) b)

Figure 30. Time history at the center of a mild steel plate a) deflection b) permanent maximum deformation (Spring back model)

This study's numerical results are in good agreement with the experimental results, differing only by 4.1% from the average indentation depth (0.84 mm) and 8.1% from the average indentation diameter (18.5 mm) observed by Somasundaram (2013).

6.2.5. Validation of the study of Sun et al.

Using the test results conducted by Sun et al. (2015), the last case in validation is considered in order to enhance the validity part of this study. This experimental study focused on building roofs by utilizing relevant impact conditions regarding hail size and terminal velocity.

Based on the simulation environment, the reaction force-time history generated by 62.5 mm diameter hail at a terminal velocity of 32 m/s is recorded and compared with the test data as shown in Figure 31.

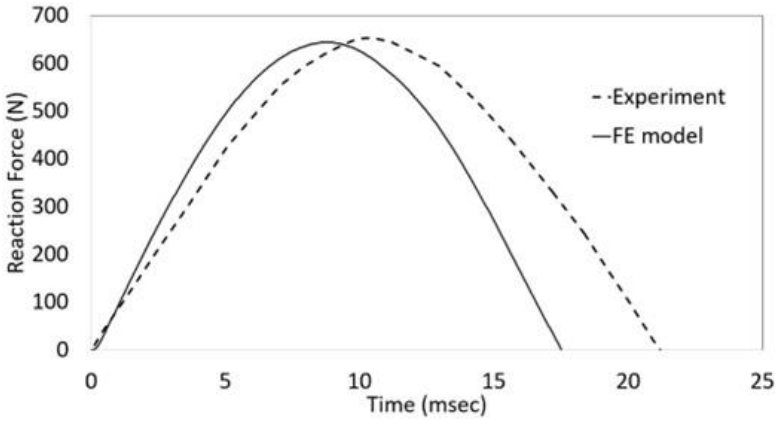

Figure 31. Comparing 62.5 mm diameter hail at a terminal velocity of 32 m/s with those presented by Sun et al. (2015)

Predicted peak forces remain below 1%, while observed differences in time intervals remain below 15%. Furthermore, numerical simulations of hail impacts within the low-velocity range were confirmed to be accurate.

6.2.6. Validation of Perera

The results of Perera (2017) can also be considered as validation. The deflections from the centre of the plate are shown in Figure 32 as a time history plot for the validation of Perera (2017). According to the current study, the finite element results agree well with the experimental results of Perera (2017). Figure 33 illustrates the contours of the deflection obtained from FE analyses at different time intervals.

According to the findings from the quasi-static tests conducted by Perera (2017), the maximum deflection occurs only at the maximum contact force. At the time when the contact phase of the impact was not yet completed, the deformation area was highly concentrated, as shown in Figure 33.

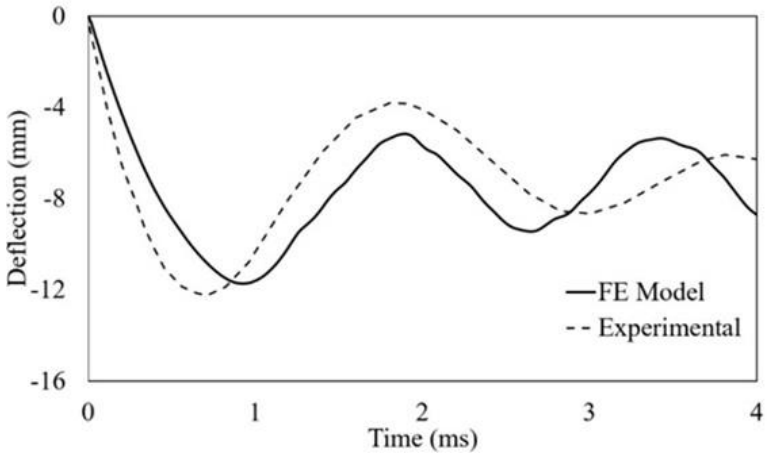

Figure 32. The deflection time history for the aluminum plate given by Perera (2017) with FE model

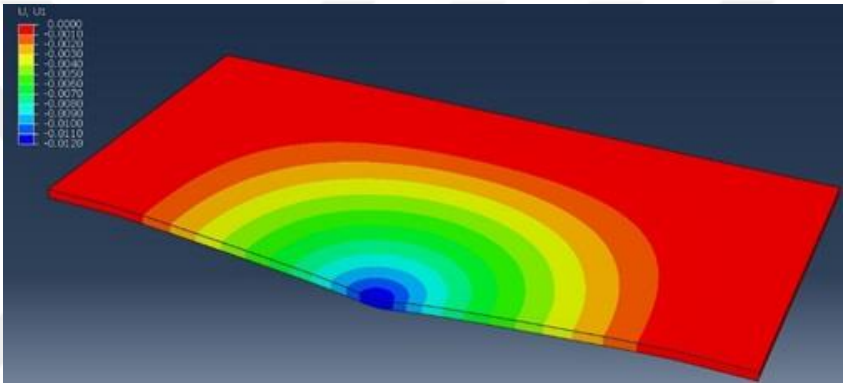

a) t = 0.92 ms (maximum deflection at peak contact force)

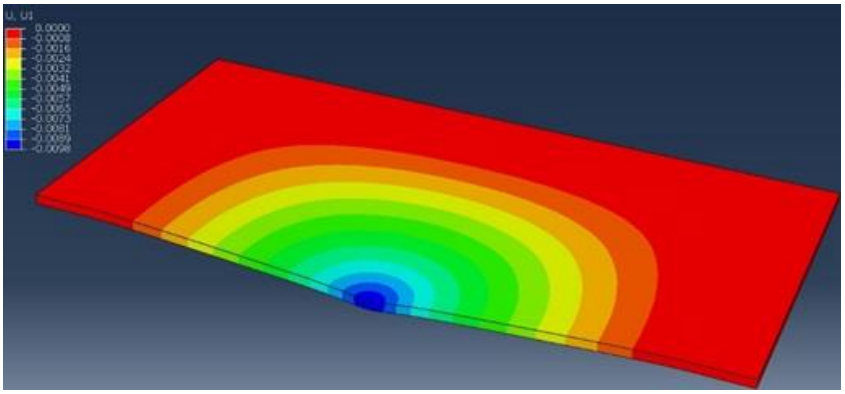

b) t = 1.26 ms (at the expiry of contact phase)

Figure 33. Deflection contours at different time steps

6.3. Finite Element Model

There is a combination of experimental and theoretical analysis in this thesis. At the end of the analytical study, the proposed equation is presented. As a result, experimental and analytical results were validated with the results of the Finite Element Model. As mentioned previously, previous finite element studies and models were analyzed. In the previous section, these models were explained. Different researchers used different programs to create finite element models. This study uses ABAQUS 2020 to model hailstones. The most important criteria for creating successful models are material properties. Hailstones must therefore be examined in terms of their material properties. In the experiment, steel sheet of grade G300 was used as the target. This target is represented as a solid extrusion in finite element models. The plate is deformable. There is a difference between this part and the study of Tippmann (2011). Figure 34 shows the plate that was used in the experiment. The plate measures one meter in height and width. The thickness of these plates is 0.30, 0.45, 0.60, 0.70, 0.80, and 1 mm. Ten artificial hailstones were used in the experiment to impact each plate. A hailstone impacts the center of the plate in the finite element model. Hailstone modeling is another important component of the finite element model. In addition, other finite element models were analyzed.

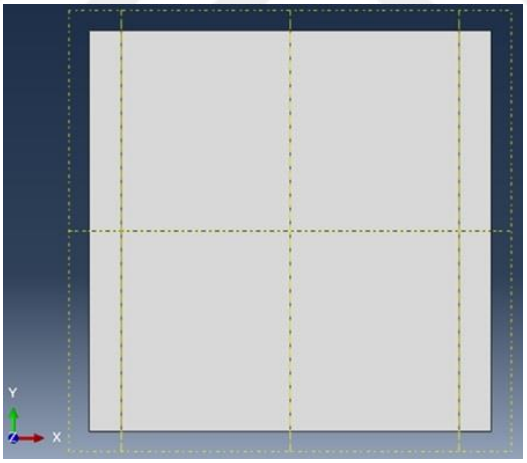

Figure 34. A plate created using ABAQUS 2020

This study was guided by Tippmann's (2011) study of hailstone impact. The hailstone was modeled as a solid revolved object. An artificial hailstone was created by creating a model hemispherical sketch using a quarter revolution. According to Figure 35, a hemispherical sketch with a quarter revolution is shown for a hailstone with a diameter of 50 mm. Having modeled the quarter of the hailstone, datum points were placed on the sketch.

Table 5 provides a definition of these points. Tippmann (2011) provided these points for the hailstone with unit diameter. These datum points were calculated for each hailstone diameter. Figure 36 shows the datum points for hailstones with a diameter of 50 mm. Using these eight datum points, quarters of the hailstone were partitioned as shown in Figure 37. A box was created inside the hailstone after it had been partitioned.

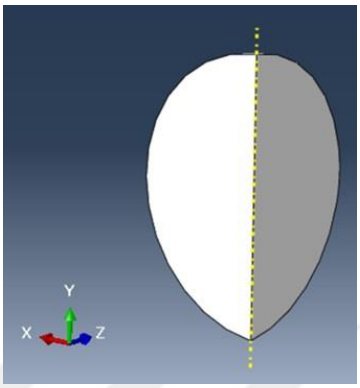

Figure 35. The hemispherical sketch of a hailstone with a diameter of 50 mm and a quarter revolution

Following the creation of the inner box, these points were projected onto the exterior surface of the sphere. These datum points were used to partition the sketch. As shown in Figure 38, the sketch has been partitioned. The mesh for the hailstone and plate is critical to the analysis. As a result, the validation part of the current study is also very important.

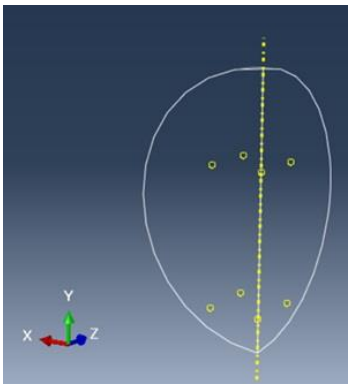

Figure 36. Datum points on hailstone with a diameter of 50 mm

As a result of the validation process, biased mesh was determined to be the most appropriate mesh for use in this study. For a hailstone with a diameter of 50.8 mm, the smallest element is 0.354 mm.

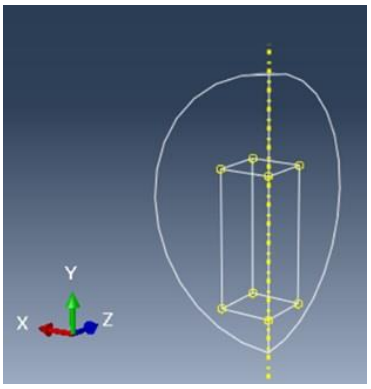

Figure 37. Hailstone inner box

Figure 22 and Figure 24 show that mesh density increases in the direction of impact on hail. Close edges to the impact point edges are divided into more parts than other edges.

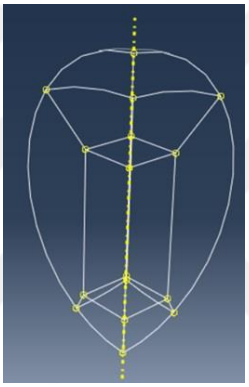

Figure 38. Partititon of the hailstone

Table 5. Datum points for unit diameter (Tippmann, 2011)

Point	X	Y	Z
1	0	0.125	0
2	0	0.65	0
3	0.2	0.125	0
4	0.2	0.65	0
5	0	0.125	0.2
6	0	0.65	0.2
7	0.2	0.125	0.2
8	0.2	0.65	0.2

A material input for the hailstone is shown in Table 6. When all these steps have been completed, a quarter of the hailstone has been transformed into a complete hailstone.

Table 6. Materials input

Line#	Contents for input file
1	*Material, name=ice
2	*Density
3	1044.95,
4	*Elastic
5	9.38e+09, 0.33
6	*Plastic
7	5.2e+06,0.
8	5.2e+06,1.
9	*TENSILE FAILURE, SHEAR =BRITTLE, PRESS= DUCTILE
10	5.17e+05
11	*Rate Dependent, type=YIELD RATIO
12	1, 0
13	1.01, 0.1
14	1.26702, 0.5
15	1.38202, 1
16	1.64903, 5
17	1.76403, 10
18	2.03105, 50
19	2.14605, 100
20	2.41306, 500
21	2.52806, 1000
22	2.79508, 5000
23	2.91008, 10000
24	3.17709, 50000
25	3.29209, 100000
26	3.55911, 500000
27	3.67411, 1000000

To conduct the experiments, artificial hailstones of 38 mm, 45 mm, and 50 mm were made. Therefore, these hailstones have been modeled based on their diameter. In the experiment, two timber battens were used to secure the steel sheet to the protective unit. A finite element model of this batten is also available. The dimensions of the timber batten are one meter in length and eight centimeters in height. Similar to the plate part batten created with solid extrusion.

To perform a finite element analysis, the material properties of the hailstone are crucial. Therefore, collecting the material properties of the hailstone is an important part of this study. As a result of hailstone formation, the density of the hailstone differs from the density of ice. The impact force of hailstones on a rigid plate was studied by Tippmann (2011).

It is also important to note that this study includes the important properties of the hailstone's material properties. Tippmann (2011) explains that in Abaqus, the ice material model consisted of a simple elastic-plastic behavior with a failure criterion based on tensile hydrostatic pressure.

It was reported in the literature that the plastic yield stress was subject to strain rate dependency based on dynamic compressive strength data. Earlier models (Kim and Keune, 2007; Park and Kim, 2006), which used the values given by Petrenko and Whitworth (1999) were selected for the ice. Former studies have used DYNA3D and LS-DYNA to calculate the elastic properties of shear or bulk modulus, but Abaqus was used to calculate Young's modulus and Poisson's ratio.

Using the isotropic relationships between the elastic constants, Poisson's ratio was calculated. Before the start of the impact tests, the diameter and mass of each hailstone were measured. Following the measurement of these values, the density of the hailstone was calculated. Finite element models use these values. This study differs from Tippmann (2011) study on density. In this study, it was recommended that 900 kg/m^3 be used. The current study used exact density values. Tippmann (2011) also provides yield strength ratio values as another important property. At the end of the study, three types of yield strength ratios were presented.

The strength ratios were compared with the impact forces. There are three categories of strength ratios: lower, average, and higher. Based on the comparisons, it was found that when lower strength ratios were used, simulation results and experiment results matched better than when upper and average strength ratios were used. In the current finite element model, a lower strength ratio was used based on that result. Table 7 provides the lower strength ratio. Tippmann (2011) provides an upper strength ratio in Table 8, however, the results obtained by using this ratio are not comparable to the experimental results. The average strength ratio is the third strength ratio. Similar to the upper yield strength ratio simulation results, using the average strength ratio did not match the experiment results. Table 9 shows the average strength ratio.

Table 7. Lower Yield Strength Ratio

Stress Ratio	Strain Rate (s^{-1})
1	0
1.01	0.1
1.267017189	0.5
1.382015232	1
1.649032421	5
1.764030465	10
2.031047654	50
2.146045697	100
2.413062886	500
2.52806093	1000
2.795078118	5000
2.910076162	10000
3.177093351	50000
3.292091395	100000
3.559108583	500000

Tensile failure is another parameter that can be used to determine hail. In Tippmann's (2011) study, three parameters related to tensile failure pressure were examined.

Table 8. Upper Strength Ratio

Stress Ratio	Strain Rate (s^{-1})
1	0
1.01	0.1
1.719300708	0.5
2.029086661	1
2.748387369	5
3.058173322	10
3.777474029	50
4.087259982	100
4.80656069	500
5.116346643	1000
5.835647351	5000
6.145433304	10000
6.864734012	50000
7.174519965	100000
7.893820672	500000

The results of the test indicated that the magnitude of the tensile failure pressure of 517 KPa best matched the experimental results. For this reason, the magnitude of the tensile failure pressure was accepted as 517 KPa in the present study. Different thicknesses of steel sheets were used for the target in the dynamic impact tests.

The impact test was conducted using G300 steel sheet. Density of steel is 7.85 kg/m^3. Elasticity modulus of steel is equal to 200 GPa. Yield stress of the steel sheet is 320 MPa.

Table 9. Average Yield Strength Ratio

Stress Ratio	Strain Rate (s^{-1})
1	0
1.01	0.1
1.495577759	0.5
1.709011483	1
2.204589242	5
2.418022966	10
2.913600725	50
3.127034449	100
3.622612208	500
3.836045932	1000
4.331623691	5000
4.545057415	10000
5.040635174	50000
5.254068897	100000
5.749646657	500000

For the laboratory test, timber battens were used to fix two edges of the steel sheet. The properties of the timber material determine the properties of the batten. The traditional Lagrangian mesh was used to develop the model and perform the correlation, as most of the forcing pulse occurs before the mesh becomes sufficiently distorted to cause significant numerical problems. Linear elements with reduced integration were chosen to model hail and slabs in Abaqus/Explicit. The stability of the solution in Abaqus/Explicit depends on the time increment (the time increment must be smaller than the critical time increment). A stable time increment was influenced by the smallest element in the model in Abaqus/Explicit. To achieve a faster calculation time, uniform elements should be included in the model.

Due to symmetry, the slab and hail can be modelled as one quarter of the scale model in the validations. However, scale models are used in the tests to avoid deformation and instability problems caused by the impact, as shown in Table 10. Another important model detail is the contact (interaction) settings and bulk viscosity.

There is a hard and frictionless contact between the outer surface of the hail and the target surface. The top sides of the plate were constrained by the batten, similar to the experiment, and the boundary conditions for these parts were fixed. These parts were prevented from rotating or moving. In Abaqus, Dynamic Explicit was selected for the impact. The linear bulk viscosity is set to 1.2 and the quadratic bulk viscosity is set to 0 in Table 11.

Table 10. Interaction property

Line#	Contents for Input File
1 2 3 4	*Surface Interaction, name=IntProp-1 *Friction 0., *Surface Behavior, pressure-overclosure=HARD

A springback analysis was performed in this thesis for the finite element analysis. After impact, the plate in the model continues to vibrate. To prevent these oscillations, a springback analysis was performed. The springback depth was measured by creating a path between one edge and the other edge of the plate due to vibration.

Table 11. Bulk viscosity input (Tippmann, 2011)

Line	Contents for input file
1 **2** **3** **4** **5**	*Step, name=Step-1 *Dynamic, Explicit , 0.0024 *Bulk Viscosity 1.2,

Compared to other measurements, springback analysis gives better results. The dent depth determined with finite element analysis is similar to the dent depth determined with finite element analysis. Without a springback analysis of the dent depth, which is measured when the vibration stops, the results between these values do not match. A path for measuring dent depth is created by selecting the fixed edge and creating the path. Reference points at the fixed edges should be assumed for measuring the indentation depth. For this reason, a path was created between the two fixed edges in this study. During the experiments, these edges were prevented from moving.

The impact points are deepest at these points. Figure 39 shows a steel sheet is a target in finite element analysis. This impact simulation is followed by a springback analysis. Figure 39 illustrates the displacement in the transversal direction following the springback analysis. Between these two black points, paths were created with selected points. The dent depth was then measured.

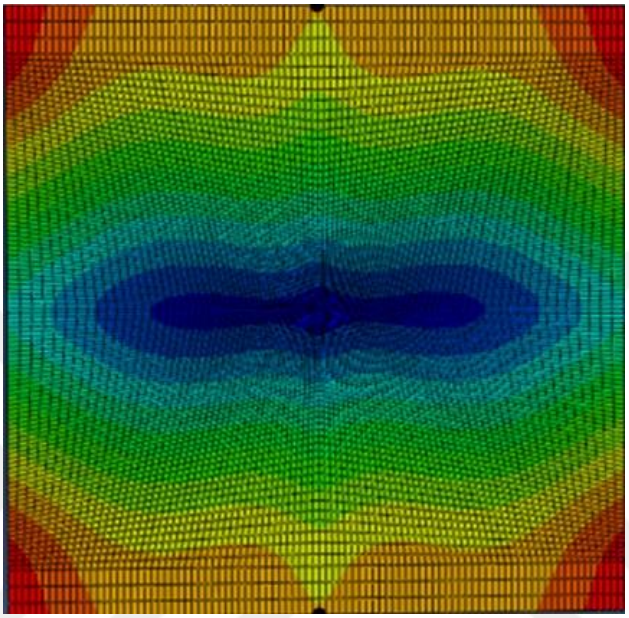

Figure 39. After Springback analysis for plate displacement

7. LIMITATIONS OF THE CURRENT STUDY

Analytical, experimental, and finite element analysis are included in this study. However, there are some limitations to this study. The first limitation relates to steel sheets. There is a difference between the nominal thickness of the steel sheets and the actual thickness provided by the factory. To overcome this problem, twelve points on each steel sheet were measured in order to calculate the average thickness. The yield stress of the steel sheet provided by the factory was used. The pressure was taken as 320 MPa. In the current experiments, all impacts were applied perpendicular to the plate. The angle of the plate is equal to zero degrees. In future studies, angles can be applied to impact tests. In addition, only steel sheets were used in the experiments. Future studies will use a variety of materials.

The plates were mounted in the protective unit prior to the start of the experiment. On two pieces of timber parallel to the ground, they were bolted. There were often incorrectly drilled bolt holes in the plates, so they were clamped using square metal pieces attached to the timber with bolts. The plates were rotated since launching hail from the top caused problems for sensors, but they were generally stable only in one orientation. The measurement of dent diameters and dent depths is another limitation of this study. A digital caliper and a depth caliper were used to measure the diameter and depth of the dent. It was known as the gauged method. The 3D scanner was utilized by Wu (2018) to measure dent depth and diameter. It was possible to reduce measurement errors by using this type of device.

8. RESULTS

Three methods of analysis were used in this thesis. The laboratory of Adnan Menderes University has developed two different methods for the preparation of artificial hailstones. There are two methods for the addition of PVA and the use of liquid nitrogen. A proposed equation was presented at the end of the study. In this study, only the dents caused by the ice balls with PVA and liquid nitrogen are reported, which remained intact after impact. The properties of the artificial hailstones are compared with those of the natural hailstones in Table 1. It has been shown that the liquid nitrogen hailstone can reproduce the properties of the natural hailstone. Several researchers have attempted to develop an equation for the depth of damage caused by the impact of hailstones. Nevertheless, the results of these studies were not able to predict dent depths that were close to the experimental dent depths. As shown in Figure 40 the impact tests performed with PVA hailstones with a diameter of 50 mm are compared with the proposed equation based on dent depths in steel plates of different thickness. The tests were labelled as follows: number of plates (number of repetitions)/ steel thickness (mm)/ average velocity (m/sec). Two different methods were used to check the velocity. The sensors are force sensors and high-speed cameras. For hailstones with an average diameter of 50.22 mm and an average mass of 64.25 grams, the final velocity is 31 m/sec. When launched from the air tank, this velocity is well matched with the pressure corresponding to the velocity. Therefore, each test label contains the average value between the speed of the radar camera and the speed of the sensor.

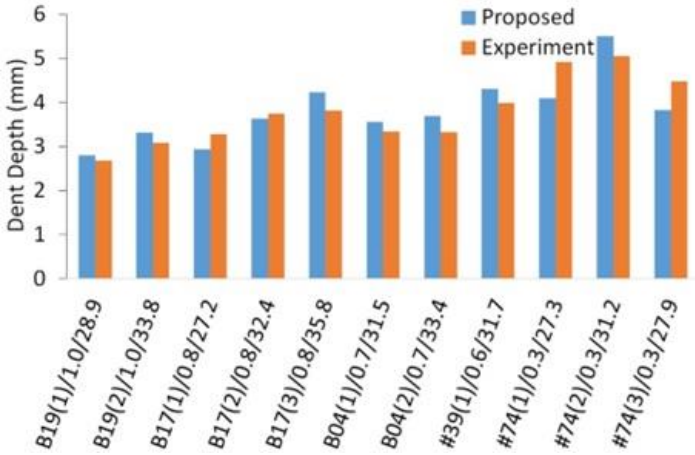

Figure 40. Results of experimental impact tests involving hailstones with a diameter of 50 mm and the equation proposed in this thesis

The ratio of the observed dent depth for each test to Eq. 23 becomes a mean professional factor equal to 0.98 with a coefficient of variation (COV) of 0.094. In the proposed equation, the dent depth of the three samples is underestimated by 14% (i.e. 1/1.16 for specimen #74(2)). The discrepancy between the determined camera velocity (V_c) and sensor velocity (V_s), or the lower average velocity (V_a) is responsible for this result. Figure 41 shows liquid nitrogen hailstone with the diameter of 45 mm. These artificial hailstones have diameters ranging between 40 and 49 mm and an average mass of 46.2 grams. In the production of the artificial hailstones, it was difficult to produce hailstones of a certain size.

Novel aspect of this study is that the experimental results are in good agreement with the theoretical findings. The dent depth caused by hailstone impact on the roofing sheet is not inversely proportional to the square roots of the sheet thickness or the yield stress caused by the vibration. In spite of the fact that the mean professional factor is not close to unity, the coefficient of variation (COV) of 0.065 found by Figure 41 is significantly lower than the coefficient of variation found by Figure 40 for 50-mm hailstones. All specimens in Figure 41, with the exception of specimen #yf=#dl (2) in Figure 41, with the exception of specimen #yf=#dl (2), show an overestimation of dent depth by up to 12% (i.e. 1/0.89 for specimen B13(5)) with a mean professional factor of 1.04. For the specimen #yf=#dl (2) velocity was computed at 29.59 m/sec, which is almost the same as the corresponding terminal velocity. Figure 42 compares dent depths on all G300 steel samples to impacts caused by 37.7 m PVA hailstones with an average mass of 27.5 grams.

Based on the results of the tests, it can be concluded that the theoretical values for the 0.3 mm steel samples are in good agreement with the experiment results. The magnitude of dent depth as well as the general trend observed in the study were closely monitored. Dent depths on 0.3 mm thick steel sheets were overestimated by 37.5 mm hailstones, which were observed to be around 0.2 mm.

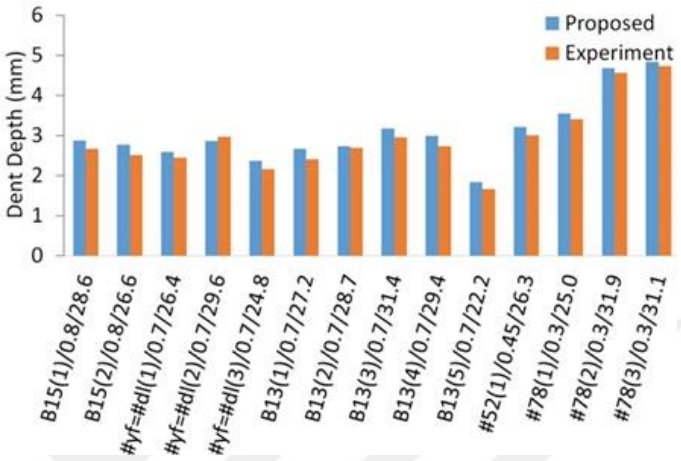

Figure 41. An experiment with liquid nitrogen hailstones with a diameter of 45 mm and a proposed equation

As with the 0.3 mm steel sheet, the dent depth was overestimated by the theory for the 0.6 mm thick steel sheet. However, the denting observed in these tests is small or did not occur. In Table 12, the proposed equation given in Eq.23 is validated with the results of experimental tests conducted by Wu (2018). Wu (2018) measured dent depths with a gauge and a 3D scanner. In the present study, some results of Wu (2018) are compared with results of FE models.

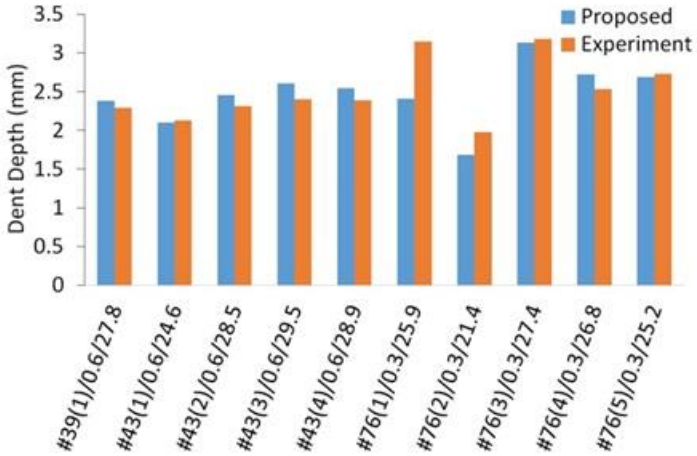

Figure 42. Tests conducted with 38 mm PVA hailstones and equation proposed

Wu (2018) refers to test numbers as hail diameter-bar pressure-repeat number (i.e. 50-10-1). The hailstones shown in Table 12 are all intact. After impact, none of the pieces were broken. Dent depth, measured using a 3D scanner by (Wu, 2018), and obtained using the proposed equation in the present study are well matched. Especially for hailstone impacts with diameters smaller than 40 mm, the proposed equation overestimated dent depth, as shown in Table 12. For the rest ones, Eq. 23 significantly underestimates the depth of the dent. To maintain consistency with Wu (2018), this study uses the values given by Wu (2018) for the parameters of the proposed equation when available; otherwise, the nominal values (such as β) obtained through experimental tests in this study are used.

According to Wu (2018) , the dentition depths measured with the gauge and the 3D scanner were not similar. A 3D scanner measured dent depth differently from a gauge. The equation predicts dent depths well in agreement with experiment measurements. When specimens are subjected to impact energy greater than 25 joules, finite element models (FE) overestimate the dent depth. Except for samples with hailstones of 25 mm, the results of the FE models do not even match those obtained using measuring equipment or 3D scans. FE results for sample 50-15-1 are shown in Figure 43. The hailstones were not able to penetrate the steel sheet. As shown in Figure 43a, there was a deflection in the cross- section of the sheet at the point of impact. The deflection of the steel sheet continues after reaching the maximum contact force until the maximum contact between the hailstone and the sheet is reached. Figure 43b shows the permanent deformation of the 0.55 mm steel sheet. In FE model, the dent depth of 4.69 mm was well matched with that obtained by the proposed equation in this current study and the experimental test conducted by Wu (2018), as the dent depths were 4.84 mm in both cases. The specimen reached the maximum contact force earlier than the maximum contact area. As can be seen in Figure 44, this is the case. Table 13 shows these comparisons. In this test, a hailstone with a diameter of 50.2 mm struck a steel sheet with a thickness of 0.55 mm at a velocity of 35.6 m/s.

Table 12. A comparison of Wu (2018) 's impact test results with the proposed empirical equation

Test number	t *mm*	D_h *mm*	Mass *gram*	V_c *m/s*	Dent Depth *mm*		Rate
					3D scan	Eq. 23	
50-10-1	1.00	51.3	66.9	30.7	3.12	3.27	0.95
50-15-2	0.75	51.8	66.5	35.2	4.25	4.43	0.96
50-15-3	0.75	50.6	62.4	35.6	4.30	4.36	0.99
50-10-1	0.75	50.8	67.3	28.7	3.51	3.51	1.00
50-10-2	0.75	51.3	66.7	31.1	3.61	3.84	0.94
50-5-3	0.75	51.2	65.2	22.7	2.25	2.46	0.91
50-4-3	0.55	51.5	66.2	26.1	3.40	3.20	1.06
50-15-3*	0.55	51.2	67.0	36.4	5.00	5.11	0.98
50-10-3	0.55	50.3	61.4	31.2	4.57	4.01	1.14
50-10-2*	0.55	50.4	64.1	28.4	4.26	3.62	1.18
45-5-3	1.00	43.9	44.6	23.7	1.96	2.00	0.98
45-10-1-1	0.75	46.2	47.2	29.0	2.96	2.99	0.99
45-9-3	0.75	45.9	46.1	28.1	2.89	2.84	1.02
45-5-2	0.75	45.2	45.3	26.8	2.57	2.67	0.96
45-14-3	0.55	45.2	46.0	34.0	3.75	3.95	0.95
45-10-3	0.55	46.1	48.1	29.8	3.59	3.40	1.06
45-10-1	0.55	44.0	44.8	31.8	3.67	3.62	1.01
38-12.5-3	0.75	37.9	27.0	35.2	2.76	2.90	0.95
38-7.5-2-2	0.75	38.7	29.0	20.0	1.60	1.47	1.09
38-7.5-3	0.75	38.0	26.1	30.2	2.28	2.38	0.96
33-6-2	0.75	33.2	19.0	24.6	1.49	1.62	0.92
33-3-1	0.75	33.2	18.7	21.4	1.39	1.35	1.03
38-7.5-3*	0.55	38.4	26.9	29.0	2.97	2.51	1.18
38-7.5-2	0.55	37.5	28.0	26.9	2.34	2.37	0.99
38-7.5-1	0.55	38.2	27.0	27.9	2.74	2.40	1.14
38-4-3	0.55	37.7	26.6	22.2	1.68	1.73	0.97
38-12.5-3	0.55	36.9	25.1	37.7	3.50	3.36	1.04
38-12.5-1	0.55	38.7	30.5	30.6	3.27	2.90	1.13
33-3-3	0.55	32.0	18.1	23.4	1.83	1.64	1.12
33-3-2	0.55	32.1	19.1	20.5	1.60	1.41	1.14
33-3-1	0.55	31.9	17.8	22.9	1.77	1.57	1.12
33-11-3	0.55	31.1	16.9	34.0	2.48	2.50	0.99
33-11-2	0.55	32.5	19.3	34.9	2.97	2.74	1.08
25-6-1	0.75	24.5	08.9	25.9	1.17	1.23	0.95
Mean							**1.03**
COV							**0.077**

The hailstones were not able to penetrate the steel sheet. As shown in Figure 43a, there was a deflection in the cross-section of the sheet at the point of impact. As shown in Figure 43a, the deflection of the steel sheet continues after reaching the maximum contact force until the maximum contact between the hailstone and the sheet is reached. Figure 43b illustrates the permanent deformation of the 0.55 mm steel sheet. In FE model, the dent depth of 4.69 mm was well matched with that obtained by the proposed equation in this current study and the experimental test conducted by Wu (2018), as the dent depths were 4.84 mm in both cases.

Table 13. Comparison of impact test results conducted by Wu (2018) with the present FE models

Test number	**t** *mm*	D_h *mm*	**Mass** *gram*	V_c *m/s*	**Dent Depth** *mm*				**Impact Energy** *Joule*	V_R *m/s*
					Gauge	**3D scan**	**Eq. 23**	**FEM**		
50-15-2*	1.00	50.7	65.8	36.2	3.30	3.75	3.92	4.41	43.1	2.1
50-10-3*	1.00	50.0	64.6	29.2	2.20	2.48	2.68	3.12	27.5	2.1
50-15-1*	0.75	50.8	66.1	34.8	4.05	4.70	4.39	4.92	40.0	1.5
50-15-1	0.55	50.2	63.2	35.6	3.90	4.84	4.84	4.69	40.0	1.9
50-15-2*	0.55	50.2	64.0	36.5	3.90	4.85	5.03	5.08	42.6	2.0
50-4-1	0.55	47.9	59.7	18.4	1.40	1.76	1.66	1.11	10.1	1.0
50-4-2	0.55	49.0	62.0	22.4	1.60	2.07	2.29	2.08	15.6	1.8
45-14-2	0.55	45.2	47.8	34.3	3.75	4.08	4.09	4.83	28.1	1.3
45-5-1	0.55	44.9	46.3	19.6	1.50	1.79	1.55	1.17	8.9	0.8
45-4-3	0.55	44.8	46.0	22.2	2.55	2.98	2.17	2.85	11.3	2.1
38-12.5-2	0.55	38.1	27.8	33.5	3.30	3.28	3.07	2.39	15.6	1.5
38-4-2	0.55	38.0	26.9	19.3	1.25	1.72	1.35	1.04	5.0	0.5
38-4-1	0.55	37.8	27.1	18.6	1.25	1.67	1.28	0.98	4.7	1.7
33-11-1	0.55	33.3	19.1	37.1	2.70	3.10	2.90	2.54	13.1	0.8
33-6-3	0.55	32.5	18.3	26.1	1.90	1.88	1.88	1.61	6.2	1.5
25-6-1*	0.55	25.5	9.2	32.8	1.35	1.74	1.79	1.41	4.9	2.4
25-6-3	0.55	26.3	9.9	32.1	1.40	1.68	1.81	1.44	5.1	0.9
25-3-4	0.55	26.3	10.2	16.1	0.50	0.72	0.74	0.68	1.3	0.4

The specimen reached the maximum contact force earlier than the maximum contact area. As can be seen in Figure 44 , this is the case.At 0.37 ms, the maximum contact force is reached, but the hailstone moves further in the loading direction at 0.91 ms, as shown in Figure 44b. As shown in Figure 44a, the hailstone and steel sheet stick together for 1.5 ms. In addition, the 50.2 mm hailstone deformed during impact, resulting in 552 mm^2 contact. The most important variable in predicting the contact force of the local indentation is the energy conversation, which includes the elastic force diagram and the stress-strain diagram of the steel sheet for the vibration and plastic energy of the material. Based on this calculation, the vibration energy in Eq. 23 is independent of time. The linear behaviour of the material ends after the stress-strain diagram, followed by horizontal movement until springback begins. The material properties also include thoughness, which is independent of time. This time-independent property of the thoughness is used to calculate the plastic energy. As can be seen in Figure 45, the experimental and theoretical results agree when the thickness of the steel sheet is varied. Based on the diameter of the hailstone, Figure 45b illustrates the relationship between experimental and theoretical results.

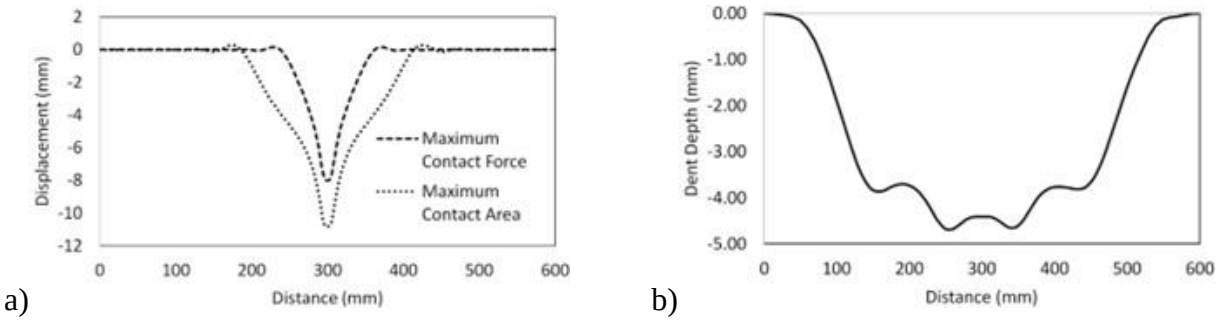

a) b)

Figure 43. FE model results of specimen 50-15-1: a) displacement during hail impact and b) final permanent deformation (springback modeling)

For thicker steel plates, the proposed equation calculates the indentation depth to be higher than the experimental result, resulting in a lower bending vibration due to the stiffer behaviour. In this thesis, the results of impact tests with liquid nitrogen and demineralised water are compared with the results of tests for pure clear ice spheres and those performed with 12% liquid PVA and 88% demineralised water. In addition, the present method was successfully carried out to produce artificial hailstone.

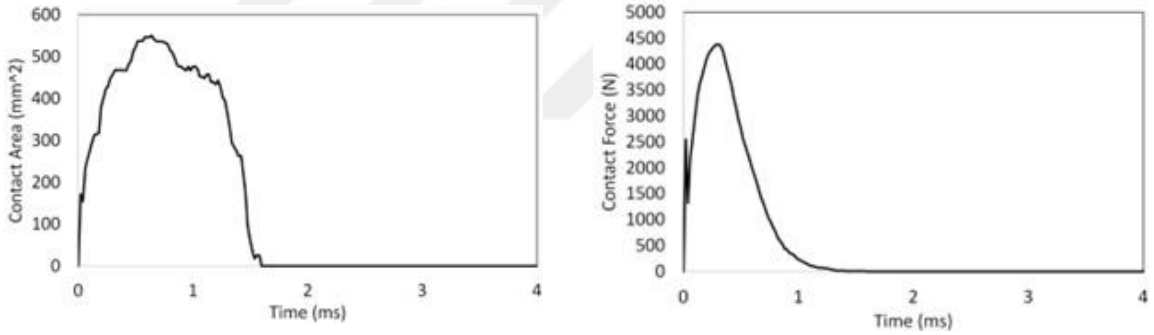

a) Contact area b) Contact force

Figure 44. Impact interaction time histories of specimen 50-15-1

According to the results of the tests with liquid nitrogen and demineralised water, the artificial hailstone showed the characteristic properties of the natural hailstone, which are listed in Table 1. The data for the impact test showing the success of integrity in impact tests are shown in Table 14.

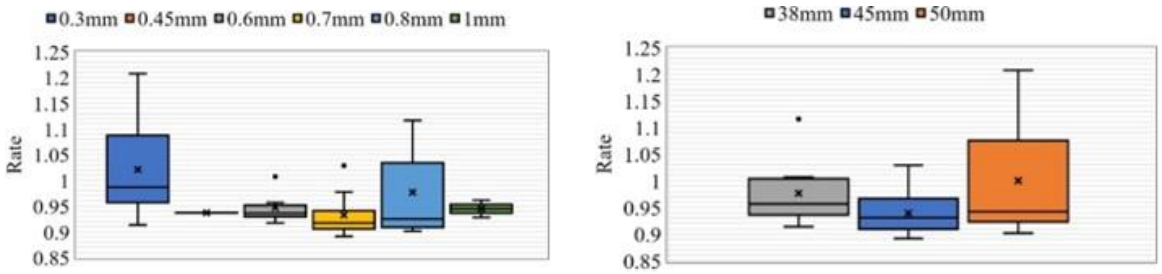

a) Based on the thickness of the steel sheeting

b) Based on the diameter of the hailstone

Figure 45. Dent depth vs. predicted depth using box whisker charts

The test results show that the artificial hailstone made from liquid nitrogen and demineralised water performs the best.

Five of the twenty-seven tests broke. A higher percentage of the artificial hailstones, almost more than half of the samples, remain intact or are only slightly shattered. This proves that liquid nitrogen and demineralised water are a good combination for simulating artificial hailstones and studying material behaviour during hailstorms.

Table 15 gives the dent depths of 45 mm diameter artificial hailstone which they are measured with gauge and the FEM analysis results. Test specimen is relabelled as steel grade/sheet thickness/ Diameter/ Shoot number. Figure 46 shows the diagrams of the impact depths of artificial hailstones with a diameter of 45 mm.

Table 14. Results of impact tests on artificial hailstones

ID	Plate thickness (mm)	Hail diameter (mm)	Pressure (bar)	Density of hailstone (g/cm3)	Velocity (m/s)		Projectile integrity
					Sensor	Camera	
1	0.30	46.50	3.20	1007.80	28.50	24.50	Whole
2	0.30	46.90	3.30	938.20	29.30	29.10	Shattered
3	0.30	47.20	3.30	979.00	34.60	29.10	Whole
4	0.30	47.90	3.30	927.40	32.30	28.50	Major Broken
5	0.30	48.90	3.30	955.30	25.10	25.70	Whole
6	0.30	46.10	3.30	949.90	40.00	33.50	Whole
7	0.30	49.40	3.30	924.30	32.70	31.50	Minor Broken
8	0.30	46.60	3.30	963.80	27.80	24.40	Major Broken
9	0.45	48.14	3.20	990.03	20.90	21.00	Major Broken
10	0.45	46.30	3.30	1053.40	26.00	27.90	Whole
11	0.45	48.72	3.30	969.20	37.70	31.90	Minor Broken
12	0.45	46.11	3.30	1006.90	27.40	31.00	Major Broken
13	0.45	47.12	3.20	996.30	24.10	26.50	Minor Broken
14	0.45	47.62	3.20	938.70	46.90	23.20	Whole
15	0.45	49.36	3.30	1005.00	111.40	31.10	Minor Broken
16	0.45	48.07	3.30	975.10	25.00	28.00	Major Broken
17	0.60	44.92	3.10	1077.60	23.30	27.40	Whole
18	0.60	49.23	3.20	989.80	22.50	25.40	Partly intact
19	0.60	48.03	3.30	1012.20	27.70	28.40	Whole
20	0.60	46.34	3.30	1088.00	24.80	29.10	Major Broken
21	0.60	48.15	3.40	997.60	26.40	29.50	Whole
22	0.60	48.83	3.40	996.50	33.80	31.00	Minor Broken
23	0.70	47.42	3.20	989.00	25.10	28.20	Major Broken
24	0.70	49.62	3.20	978.00	28.90	28.20	Shattered
25	0.70	47.33	3.30	1027.60	34.10	29.20	Shattered
26	0.70	45.23	3.30	1032.90	39.50	36.90	Shattered
27	0.70	47.12	3.20	1017.30	30.80	32.20	Shattered

The impact test was carried out on steel sheets of different thickness. Figure 47 shows the ABAQUS simulations of the test specimen G300/0.70/45/7. In this impact test, an artificial hailstone was made of PVA. Sheet steel 0.70 mm thick was used for the target.

Table 15. Dents depths of the 45mm diameter hailtone made of 12%PVA and 88% demineralized water

Test ID	t (mm)	Diameter (mm)	Mass (gr)	V_c (m/s)	D (mm) (gauge)	D (mm) (FEM
G300/0.60/45/3	0.60	43.46	46.50	33.40	3.18	2.85
G300/0.70/45/8	0.70	44.22	45.80	23.12	1.67	2.02
G300/0.70/45/7	0.70	44.71	48.90	30.06	2.78	2.70
G300/0.80/45/1	0.80	43.72	44.50	28.69	2.34	2.15
G300/0.80/45/9	0.80	44.68	45.90	27.55	2.31	2.10
G300/0.45/45/2	0.45	44.53	45.00	30.06	2.95	2.94
G300/0.45/45/4	0.45	45.17	46.40	28.69	2.94	2.91
G300/0.30/45/9	0.30	44.86	44.50	28.69	3.87	4.15

In the FEM analysis, the speed determined by the high-speed camera was used. The impact speed of the hailstone is 30.06 m/s. After the experiment, the dent depth was measured to 2.78 mm using a digital calliper. The result of the FEM analysis also showed a dent depth of 2.70 mm. The rate between them is 0.97. Figure 48 shows the simulation of sample G300/0.30/45/9.

In this experiment, the hailstone was made of PVA and demineralised water. But this time the thickness of the target plate is 0.30 mm. The diameter of the hailstone is 44.86 mm. In Figure 48, the duration of the contact between the hailstone and the plate and the simulation of the hailstone until the end of the impact can be seen. In this test, the hailstone hit the plate with a velocity of 28.69 m/s.

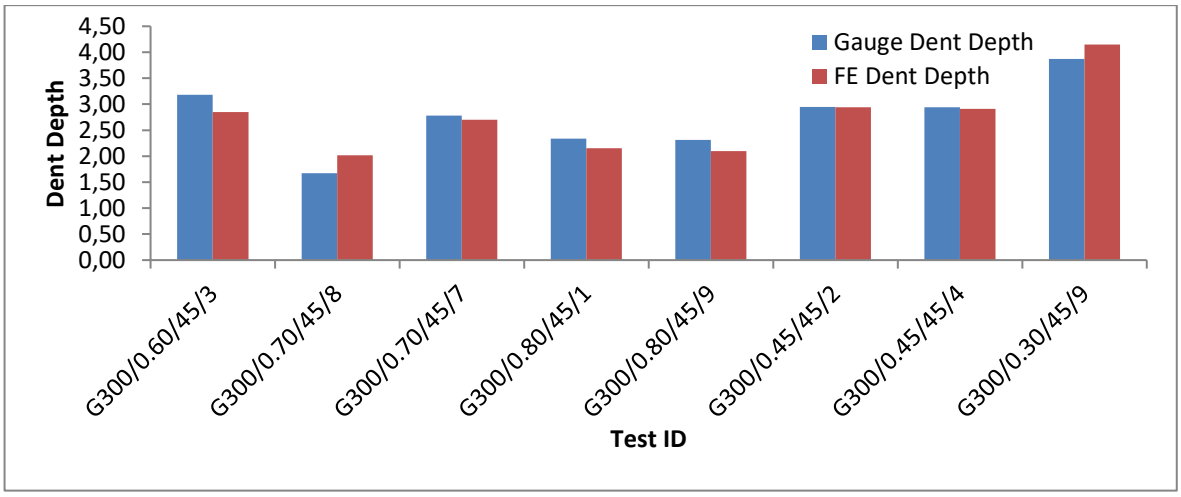

Figure 46. Graphs of the 45mm diameter artifcial hailstone made of PVA

The depth of the dent was measured with a gauge at 3.87 mm and given as 4.15 mm in ABAQUS 2020. Tests were carried out to investigate the impact of hailstones of the same diameter on steel sheets of different thickness.

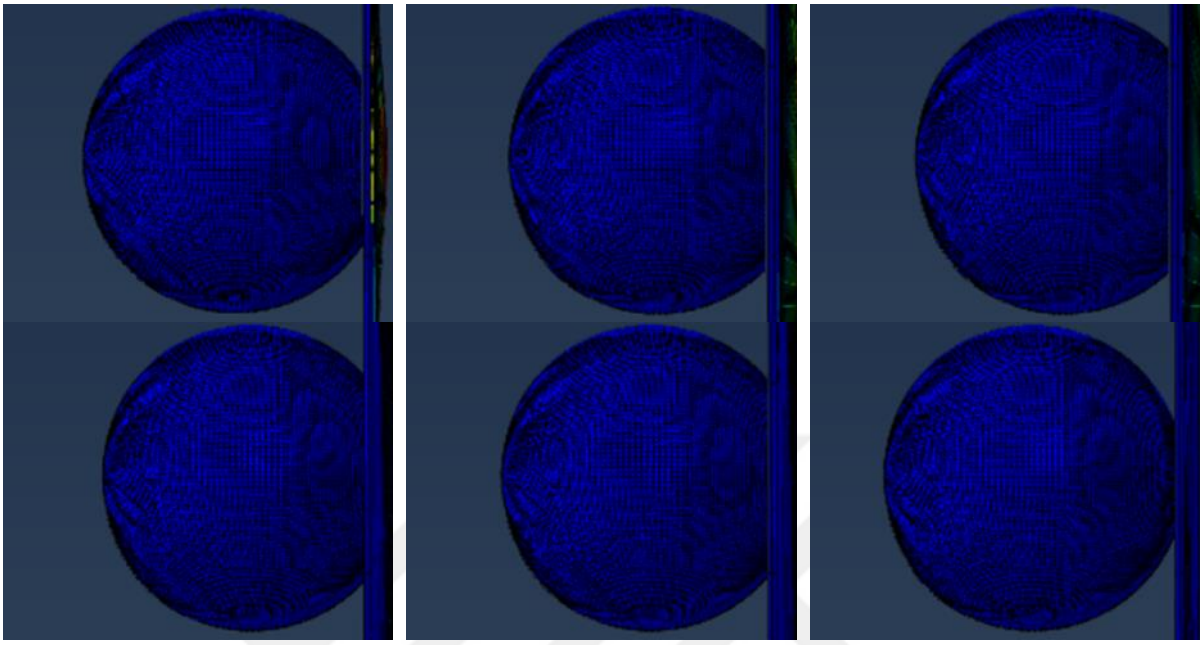

Figure 47. Finite Element simulation of Specimen of G300/0.70/45/7

The impact tests were carried out with all diameters of artificial hailstone on sheets of different thickness. Figure 49 shows the impact of the artificial hailstone with a diameter of 45 mm on steel sheets of different thickness. In these two impact tests, the diameters of the artificial hailstones are 44.73 and 44.51 mm. The terminal velocity of these artificial hailstones is 30.6 m/sec. The plate thickness is 0.70 mm and 0.45 mm. In these two experiments, almost all parameters are the same, only the plate thickness is different and in connection with this difference the dent depth is higher for the 0.45 mm thick plates than for the 0.70 mm thick plates.

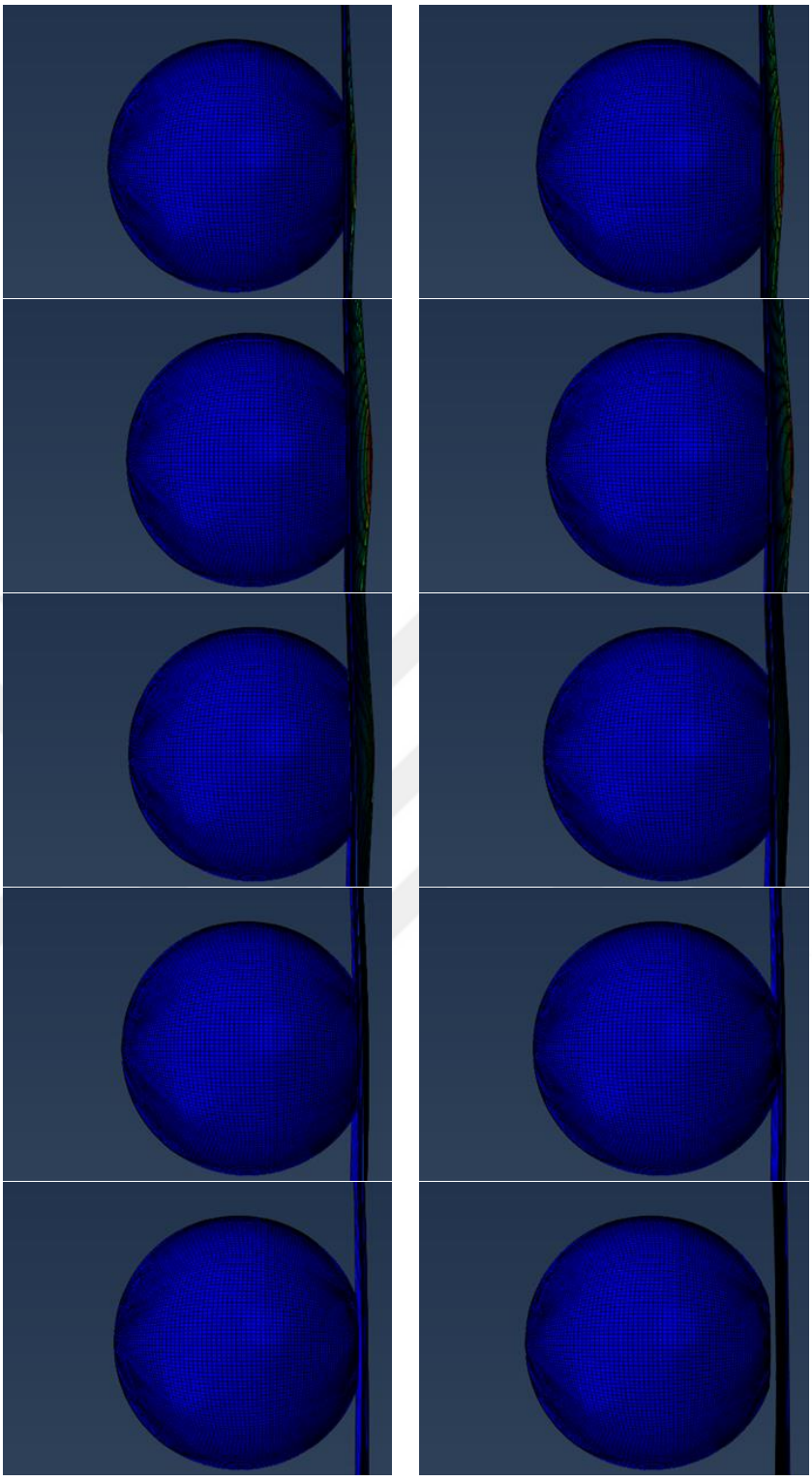

Figure 48. Impact simulation of specimen G300/0.30/45/9

In Uz et al. (2021) the indentation depths were compared with the gauge and their proposed equation. But in these results the finite element analysis is not included. In contrast to this study, finite element analysis was performed for some of these results. In the study by Uz et al. (2021), artificial hailstones of 50 mm, 45 mm and 38 mm diameter were investigated.

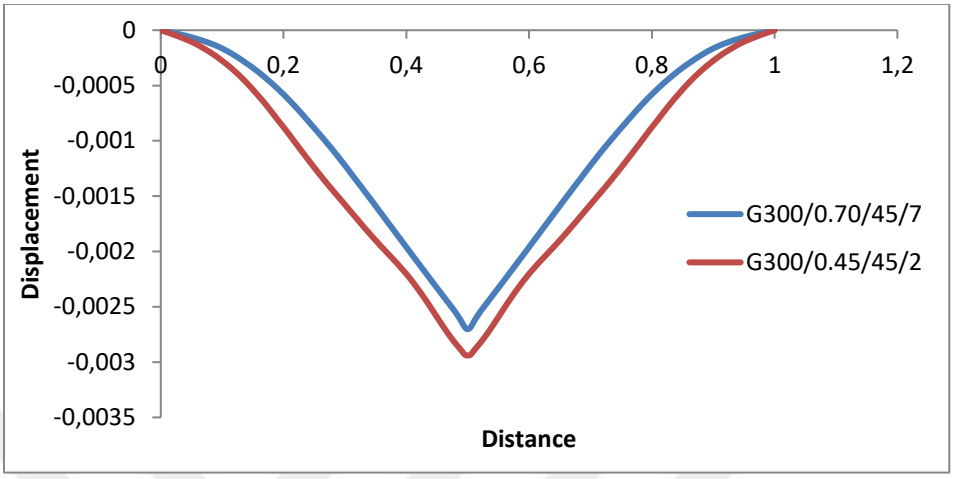

Figure 49. Graphs of displacement-distance between two specimens

The proposed equations were applied to these results in the given Table 16. The test ID consists of steel sheet (number of sheets)/ thickness of steel sheet/ average velocity. Three velocities are given in Table 16. V_s is the velocity detected by the sensors. The second velocity is V_c . This velocity was calculated by the high-speed camera. The third velocity is the average of these two velocities. But it has already been mentioned that in Abaqus V_c was used.

Table 16. Dent depth results measured with gauged, proposed and FEM

Test ID	t mm	Diameter mm	Mass (gr)	V_a m/s	V_s m/s	V_c m/s	D mm gauge	D mm Proposed	D mm FEM
B19(1)/1.00/28.99	1.00	50.58	64.6	28.99	27.92	30.06	2.68	2.79	2.7
B19(2)/1.00/33.80	1.00	50.17	63.9	33.80	30.87	36.74	3.28	3.32	3.37
B17(1)/0.80/27.26	0.80	50.25	64.1	27.26	21.46	33.06	3.27	2.93	2.93
B13(1)/0.70/27.22	0.70	44.81	47.4	27.22	25.75	28.69	2.4	2.67	2.52
B15(2)/0.80/26.59	0.80	45.59	49.3	26.59	25.86	27.33	2.51	2.76	2.24
B13(2)/0.70/28.75	0.70	43.98	44.8	28.75	25.95	31.56	2.69	2.75	2.39
#43(1)/0.60/24.60	0.60	37.39	27.4	24.60	21.87	27.33	2.13	2.11	1.95
#43(2)/0.60/28.48	0.60	37.53	27.5	28.48	28.07	28.90	2.31	2.46	2.06
#43(3)/0.60/29.59	0.60	37.45	28.3	29.59	29.12	30.06	2.4	2.62	2.19

The data from Table 16 was used to create the graph in Figure 50. These results show that there is a good correlation between the results of the first two samples. The indentation depth measured after the tests, the indentation depth predicted by the proposed equations and the indentation depth taken from the ABAQUS results are close to each other.

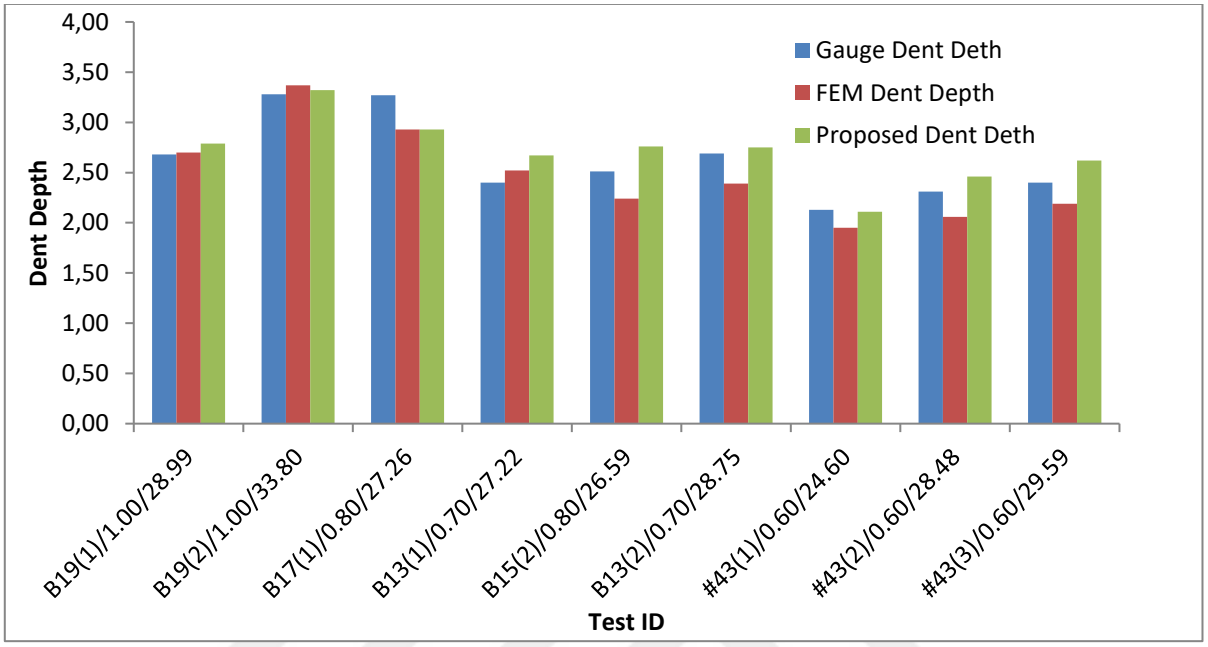

Figure 50. Dent depths measured by three methods

The first specimen is B19(1)/1.00/28.99 The depth of penetration measured with the depth calliper was 2.68 mm. It was calculated to be 2.79 mm using the proposed equation. After simulation, the penetration depth was 2.70 mm. The second sample is B19(2)/1.00/33.80. The thickness of the steel sheet is the same as the previous sample. It is 1.00 mm. The depth of the bulge is 3.28 mm. The depth is measured as 3.32 mm using the proposed equation. The results from FEM from ABAQUS give a bulge depth of 3.37 mm.

9. DISCUSSION

With the proposed equation, new knowledge could be gained about the factors influencing dent resistance of roof panels exposed to hailstorm. With the findings of this study, new methods for designing hail-resistant steel sheets can be implemented that are more widely applicable, comprehensive, and consistent with natural conditions

Velocity measurement is important for hail impact resistance. Therefore, it is important to use sensitive equipment for velocity measurement.

The experimental setup used in this study can be used more specifically to determine the hail resistance of building materials if the above limitations are improved.

Using the equation proposed in this study, the effect of the impact angle and the steel sheet profile will be studied in the future. It is important to study the hail resistance of the optimised steel profiles in detail. It is important to test different impact angles. To evaluate the hail resistance more accurately, hailstones with different diameters should be used in the future to investigate different steel sheet derived materials. Using the equation proposed in this paper, the effect of the impact angle and the steel sheet profile will be studied in the future.

10. CONCLUSION

The aim of this thesis is to validate the experimental and theoretical results using a finite element model.

This study summarized the parameters that can be used to predict the dent depth. These parameters include the impact energy, the plate thickness, the strength of the material, the distance between the battens, the distance between the nearest edge of the plate and the centre of gravity of the dent, and the hail diameter.

The effects of the hail diameter on the dent depth varies according to flexural vibration and inelastic behaviour of steel sheet. During flexural vibration, the diameter of the hailstone plays an important role in the dent depth, whereas the diameter of the hailstone has no influence on the dent depth in the case of inelastic behaviour of the steel plate.

Hailstone with different diameters can cause same permanent deformation due to impulse. If the impact energy is the same, a smaller hailstone with a higher impulse will cause a similar permanent depth as a larger hailstone with a lower impulse.

Based on the results of the experiments and the models from FE, the empirical findings agree with those observed in the experiments.

The permanent deformation found by the proposed equations is in good agreement with the observations of results obtained fromexperiments. Therefore, the calculated value of the permanent deformation in the steel roof panel was within 98% accuracy of the actual value.

This study has some difficulties, such as measuring the velocities accurately, determining the desired final velocity for each hailstone, the non-uniform thickness of the steel plate, stabilising the plate in the same way, and other shortcomings. Despite all these difficulties, the proposed equation with a lower energy was able to accurately predict dent depth in 0.3 mm thick plates with a yield strength close to 300 MPa at a terminal velocity of hailstones with a diameter of 45 mm. Steel in a limited range of thicknesses is available for the experiment.

REFERENCES

Allaby, M., and Garratt, R. (2014). Hail, Sleet, Snow. *In: Blizzards. Facts On File*, 85-92.

Anghileri, M., Castelletti, L.-M. L., Invernizzi, F., and Mascheroni, M. (2005). A survey of numerical models for hail impact analysis using explicit finite element codes. *International Journal of Impact Engineering, 31*(8), 929-944. doi:https://doi.org/10.1016/j.ijimpeng.2004.06.009

Bircan, T., Uz, M. E., Kirnak, H., Erdem, E., Goren, M., and Kop, M. D. (2018). *Investigation of a Theory for Determining Hailstone Resistance*. Paper presented at the 13th International Congress on Advances in Civil Engineering, Izmir, Turkey.

Brimelow, J. (2018). Hail and Hailstorms. In: Oxford University Press.

Brimelow, J. C., Krauss, T. W., and Reuter, G. W. (2002). Operational forecasts of maximum hailstone diameter in Mendoza. *The Journal of Weather Modification, 34*, 8-17.

Carney, K. S., Benson, D. J., DuBois, P., and Lee, R. (2006). A phenomenological high strain rate model with failure for ice. *International Journal of Solids and Structures, 43*(25), 7820-7839. doi:https://doi.org/10.1016/j.ijsolstr.2006.04.005

Chang, D. C., and Khetan, R. P. (1984). Surface Damage of Steel, Aluminum, and Chopped-Fiber Composite Panels Due to Projectile Impact. *Journal of Reinforced Plastics and Composites, 3*(3), 193-203. doi:10.1177/073168448400300302

Crenshaw, V., and Koontz, J. D. (2002). Hail: Sizing it up! *Western Roofing Magazine*.

CSIRO, and BoM. (2007). *Climate change in Australia : technical report / [CSIRO and the Bureau of Meteorology]*. Aspendale VIC: CSIRO Marine and Atmospheric Research.

Dunlop, S. (2008). Oxford Dictionary of Weather

Engelbert, P. (1997). *The Complete Weather Resource: Weather phenomena*: UXL.

Fleming, H. G., Skarajew, M., and Szalla, J. A. G. (1997). A Laboratoy Dent Test for Outer Panel Steels.

Flüeler, P., Stucki, M., Guastala, F., and Egli, T. (2008). *Hail Impact Resistance of Building Materials Testing, Evaluation and Classification*. Paper presented at the 11 DBMC

International Conference on Durability of Building Materials and Components Istanbul Technical University, Istanbul, Turkey.

Gold, L. W. (2014). Building ships from ice: Habbakuk and after. *Interdisciplinary Science Reviews, 29*(4), 373-384.

Greenfeld, S. H. (1969). *Hail resistance of roofing products* (Vol. 23): Building Research Division, US Institute for Applied Technology.

Heymsfield, A., Szakáll, M., Jost, A., Giammanco, I., Wright, R., and Brimelow, J. (2020). CORRIGENDUM. *Journal of the Atmospheric Sciences, 77*(1), 405-412. doi:10.1175/jas-d-19-0185.1

Hile, K. (2009). *The Handy Weather Answer Book*: Visible Ink Press.

Johnson, T. E., and Schaffnit, W. O. (1973). Dent Resistance of Cold-Rolled Low-Carbon Steel Sheet. *SAE Technical Paper 730528, 82*(A), 1-12. doi:10.4271/730528

Juntikka, R., and Olsson, R. (2009). *Experimental and modelling study of hail impact on composite plates*.

Kim, H., and Kedward, K. T. (1999, July 7-9 1999). *Experimental measurement and numerical prediction of hail ice impact damage on composite panels.* Paper presented at the Proceeding of The 12th International Committee on Composite Materials, Paris, France.

Kim, H., and Kedward, K. T. (2000). Modeling Hail Ice Impacts and Predicting Impact Damage Initiation in Composite Structures. *AIAA Journal, 38*(7), 1278-1288. doi:10.2514/2.1099

Kim, H., and Keune, J. N. (2007). Compressive strength of ice at impact strain rates. *Journal of materials science, 42*(8), 2802-2806.

Kim, H., Welch, A. D., and Kedward, T. K. (2003). Experimental investigation of high velocity ice impacts on woven carbon/epoxy composite panels. *Composites Part a: Applied Science and Manufacturing, 34*, 25-41. doi:10.1016/S1359-835X(02)00258-0

Kuene, J. N. (2004). *Development of a Hail Ice Impact Model and the Dynamic Compressive Strength Properties of Ice.*, Purdue University,

Laurie, J. A. P. (1960). *Hail and Its Effects on Buildings*: Council for Scientific and Industrial Research.

Leslie, L., Leplastrier, M., and Buckley, B. (2008). Estimating future trends in severe hailstorms over the Sydney Basin: A climate modelling study. *Atmospheric Research, 87,* 37-51. doi:10.1016/j.atmosres.2007.06.006

Liang, M. (2015). *Experimental investigation, development and optimisation of steel roof sheeting against the effect of hail impact.* (Bachelor Thesis), University of Wollongong, Australia.

Maguire, J. R. (2014). *Experimental Determination of The Effects of Hail Impact on Steel Building Envelopes.* (Bachelor Thesis), University of Wollongong, Australia.

Moore, D., and Wilson, A. (1978). *Photovoltaic solar panel resistance to simulated hail. Low-Cost Solar Array Project*.

Niemeier, B. A., and Burley, C. E. (1978). *Hailstone Response of Body Panels - Real and Simulated*. https://doi.org/10.4271/780398

Nomura, S., Yutori, Y., Iwaya, J., Miyahara, M., and Kokubo, I. (1984). *A study of the dynamic dent resistance.* Paper presented at the Efficiency in Sheet Metal Forming, IDDRG 13 th Biennial Congress.

Oard, M. J. (2015). *The New Weather Book*: Master Book Publishers.

Park, H., and Kim, H. (2006). Resistance of adhesively bonded composite lap joints to damage by transcerse ice impact. *American Society for Composites - 21st Technical Conference of the American Society for Composites 2006, 3*, 1187-1204.

Paterson, D. A., and Sankaran, R. (1994). Hail impact on building envelopes. *Journal of Wind Engineering and Industrial Aerodynamics, 53*(1), 229-246. doi:https://doi.org/10.1016/0167-6105(94)90028-0

Perera, S. (2017). *Modelling Impact Actions of Flying and Falling Objects.* (Doctor of Philosophy), The University of Melbourne, Melbourne, Australia. Retrieved from http://hdl.handle.net/11343/194798

Petrenko, V. F., and Whitworth, R. W. (1999). *Physics of ice*: OUP Oxford.

Ramsay, H. (2015). *Experimental investigation, development and optimization of steel roof sheeting against the effect of hail impact.* (Bachelor Thesis), University of Wollongong, Australia.

Raupach, T. H., Martius, O., Allen, J. T., Kunz, M., Lasher-Trapp, S., Mohr, S., . . . Zhang, Q. (2021). The effects of climate change on hailstorms. *Nature Reviews Earth & Environment, 2*(3), 213-226. doi:10.1038/s43017-020-00133-9

Schulson, E. M. (1999). The structure and mechanical behavior of ice. *JOM, 51*(2), 21-27. doi:10.1007/s11837-999-0206-4

Shi, M. F., Brindza, J., Michel, P., Bucklin, P., Belanger, P., and Prencipe, J. (1997). Static and Dynamic Dent Resistance Performance of Automotive Steel Body Panels. *SAE Technical Paper*.

Somasundaram, V. (2013). *The characterisation of hail and fraudulent impacts to vehicle body panels*. Retrieved from

Sun, J., Nelson, L., Lihai, Z., Dong, R., and Emad, G. (2015). Contact forces generated by hailstone impact. *International Journal of Impact Engineering, 84*, 145-158.

Swift, J. M. (2013). *Simulated Hail Ice Mechanical Properties and Failure Mechanism at Quasi-Static Strain Rates.* (PhD.), University of Washington,

Tippmann, J. D. (2011). *Development of a Strain Rate Sensitive Ice Material Model for Hail Ice Impact Simulation.* (MS), University of California, San Diego, United States.

Uz, M. E., Kop, M. D., and Yildirim, E. M. (2022). Analysis of Out-of-Plane Hail Impact Resistance of Steel Roof Panels. *Experimental Techniques, 46*(3), 509-527. doi:10.1007/s40799-022-00550-z

Uz, M. E., Kop, M. D., and Yildirim, E. M. J. A. A. (2021). Determining the empirical model for estimating the permanent deformation in flat roof panels under hail impact. *11*(12), 125117.

Uz, M. E., and Sızar, M. D. (2021). Analyzing Dent Resistance of Steel Roof Panels Subjected to Hail Impacts. *9*. doi:https://dergipark.org.tr/tr/pub/jesd/issue/64976/952121

Uz, M. E., Teh, L. H., and Maguire, J. (2014). Developing Australia's first hail-proof roofing profiles. In. University of Wollongong, Australia, Sustainable Building Research Center: SBRC Open Day 2014.

Uz, M. E., Yilmaz, G., and Bircan, T. (2017). The Making of a Hailstone Simulated Realistic Damage. *Journal of Engineering Sciences and Design, 5*(2), 411-423. doi:10.21923/jesd.327312

Vreede, P. T., Tamis, P. J., Roelofsen, M. E., and BV, H. G. (1995). *The Influence of Material Properties and Geometry on Dynamic Dent Resistance: Experiments and Simulations.* Paper presented at the Material & Body Testing: Proceedings of the International Body Engineering Conference, IBEC, Detroit, Michigan, USA.

Worswick, M. J., Finn, M. J., and Thorburn, H. J. (1997). *A numerical study of the geometric and material parameters affecting static and dynamic denting*. Retrieved from

Wu, Y. (2018). *Determining the Effects of Hailstone Impact on Flat Cold-Reduced Steel Roof Sheeting* (Master of Philosophy thesis Master of Philosophy thesis), University of Wollongong, Australia. Retrieved from https://ro.uow.edu.au/theses1/192 (https://ro.uow.edu.au/theses1/192)

Yılmaz, G., Uz, M. E., Dawood, M., and Kop, M. D. (2020). Production of Artificial Hailstone with Liquid Nitrogen and Comparisons with Other Artificial Hailstones Up to Now. *Journal of Engineering Sciences and Design, 8*(4), 1180-1189. doi:https://dergipark.org.tr/en/pub/jesd/issue/58117/672264

T.C.

AYDIN ADNAN MENDERES UNIVERSITY

GRADUATE SCHOOLOF NATURAL AND APPLIED SCIENCES

SCIENTIFIC ETHICAL STATEMENT

I hereby declare that I composed all the information in my master's thesis entitled “The Effects of Hail Impact on Steel Roofing Profiles with FEM and Laboratory Tests” within the framework of ethical behavior and academic rules, and that due references were provided and for all kinds of statements and information that do not belong to me in this study in accordance with the guide for writing the thesis. I declare that I accept all kinds of legal consequences when the opposite of what I have stated is revealed.

Meryem Dilara KOP

… / … / …

CURRICULUM VITAE

Last name, First name : KOP Meryem Dilara

Level	**Institue/University**	**Graduation Date**
Master's degree	Aydın Adnan Menderes University	-
Bachelor's degree	Aydın Adnan Menderes University	10/06/2019

Academic Publications

Published Journals indexed in SCI-Expanded

1. Uz, M. E., **Kop, M. D**., and Yildirim, E. M. J. A. A. (2021). Determining the empirical model for estimating the permanent deformation in flat roof panels under hail impact.AIP Advances, 11(12), 125117.
2. Uz, M. E**., Kop, M. D.**, and Yildirim, E. M. (2022). Analysis of Out-of-Plane Hail Impact Resistance of Steel Roof Panels. Experimental Techniques, 46(3), 509-527. doi:10.1007/s40799-022-00550-z

Published Journals indexed in TR dizin

1. Yilmaz, G., Uz, M. E., Sizar, M. D. and **Kop, M. D.** (2020). Production of artificial hailstone with liquid nitrogen and comparisons with other artificial hailstones up to now. *Mühendislik Bilimleri ve Tasarım Dergisi, 8*(4), 1180-1189.

Published International Conferences

1. Bircan, T., Uz, M. E., Kirnak, H., Erdem, E., Goren, M., and **Kop, M. D.** (2018). Investigation of a Theory for Determining Hailstone Resistance. Paper presented at the 13th International Congress on Advances in Civil Engineering, Izmir, Turkey.